Response to Reviewer 1 (RC1)

Manuscript egusphere-2026-457: "Country-wide rainfall estimates from a commercial microwave link network in Belgium", by K. Van Weverberg et al.

General response

We sincerely thank the reviewer for the thorough and constructive assessment of our manuscript, and in particular for the concrete suggestions on how to evaluate each processing step individually. These suggestions have substantially shaped the revision, which goes considerably beyond the individual points raised below. Reviewer comments are reproduced in blue italics, followed by our response and the corresponding changes to the manuscript. Where we quote from the revised manuscript, the text is given in italics between quotation marks. Since a revised manuscript cannot be uploaded during this response phase, we refer to the section, figure and table numbers of the revised manuscript throughout, and we reproduce the modified figures and tables at the end of this document, in addition to a number of figures specifically helping with this review.

Before addressing the individual comments, we note that the reviewers' suggestions prompted a substantially deeper revision of the retrieval pipeline than the individual points below might suggest, with a more thorough quality assessment of the disdrometers (leading to the removal of one instrument), a more consistent formulation of the attenuation–rain-rate relation that is fitted directly in the retrieval (R–γ) direction and compared like-for-like with previous studies, and an α-weighting of the minimum and maximum rain rates that accounts for the skewness of sub-window rainfall following Overeem et al. (2016a). Importantly, every one of these changes acted to corroborate and strengthen the central conclusion of the paper, namely that for these cases carefully processed CML rainfall matches or outperforms the operational RAD-QPE product. We summarize seven overarching changes that affect several of the responses below:

(1) Quality re-assessment of the disdrometers and revision of all results. During the revision we performed an additional quality assessment of the three disdrometers used to derive the local attenuation-rainfall (γ-R) relations. This revealed suspicious behaviour of the instrument located at Uccle: more than half of the values of its velocity-diameter matrix fell outside the range expected from the Gunn-Kinzer terminal fall-velocity relation. Consultation with the responsible RMI staff members indicated that the instrument likely requires recalibration (see also Review Figure 9. We therefore omitted this disdrometer from the analysis and refitted the power-law coefficients using the two remaining instruments (the OTT Parsivel^2 at Melle and the Thies Laser Precipitation Monitor at Liège). At the same time, the entire disdrometer processing chain was upgraded to the DISDRODB framework (Ghiggi et al., 2026), including a hydrometeor classification, filtering of non-physical velocity-diameter combinations, splashing removal, and full T-matrix scattering calculations at 1 GHz intervals (Sect. 3.5 of the revised manuscript). All CML rainfall estimates, figures and evaluation statistics in the revised manuscript have been recomputed accordingly. The revised relations predict a higher rain rate than ITU for a given specific attenuation throughout the light-rain range, where the observations are most numerous, and a lower rain rate only at the heaviest rates; the crossover intensity and the magnitude of this difference both increase with frequency, so the largest departures occur for the E-band links and in the light-rain regime (Fig. 4 and Table 4). This is consistent with the newly designed frequency×length skill evaluation

(Fig. 7), where the local log–log relation reduces the positive bias of the ITU retrieval most clearly for the short, high-frequency links. We note that Fig. 4 and Table 4 now report the relation in the retrieval (R–γ) direction (see overarching change 2 below); the corresponding attenuation-form coefficients follow by the analytic inversion $a' = \mathrm{a}^{-1/\mathrm{b}}, \quad b' = 1/\mathrm{b}$.

(2) A more consistent formulation of the attenuation–rain-rate relation, fitted directly in the retrieval direction. Acting on Comment 2.20 from Reviewer 2 about the comparison between our disdrometer fits and those from Overeem et al. (2016a), we found that our original comparison with Overeem et al. (2016a) differed from their approach in two respects. They fitted the inverse R–γ relation with an unweighted non-linear least-squares fit, whereas we had fitted the γ–R relation in log–log space. Neither the direction of the regression nor the objective function was therefore matched, and a meaningful comparison required us to reproduce both choices. We now fit the relation directly in the retrieval direction, $R = \mathrm{a} \cdot \gamma^{\mathrm{b}}$, and invert it analytically to the attenuation form ($a' = \mathrm{a}^{-1/\mathrm{b}}, \quad b' = 1/\mathrm{b}$) that pycomlink and the ITU recommendation expect, so that the comparison with Overeem et al. (2016a) is now direct. Repeating the fit with both objective functions turned out to be more than a formality: the two estimators are optimal under different assumptions about the error structure, and their coefficients diverge substantially at the lowest and highest frequencies, where the non-linear fit is dominated by the rare high-intensity samples and is markedly less reproducible between the two disdrometers. Once the same estimator as Overeem et al. (2016a) is adopted, the Belgian and Dutch coefficients at 10 GHz agree closely, which indicates that apparent differences between locally fitted relations reported in the literature can be dominated by the fitting choices rather than by climatology. Both fits are therefore retained as the L and N factor levels of the full evaluation (Table 2), and the role of the objective function is now discussed explicitly in Sect. 4.4. We additionally verified that the regression direction alone (fitting γ–R and inverting, versus fitting R–γ directly) changes the retrieved rainfall only marginally, well below the effect of the objective function.

(4) Redesign of the experiment set as a full factorial, and removal of methods developed for 30-second data. Prompted by the reviewer's general concern about methods and thresholds developed for other data formats, two methods that we used in the previous iteration, but are in principle developed for 30-second instantaneous data have been removed: the rolling standard-deviation wet-dry classification of Schleiss and Berne (2010) and the time-dependent wet-antenna scheme of Schleiss et al. (2013), both of which rely on time scales and thresholds that are not compatible with 15-minute MINMAX records. Instead, the physically based, frequency- and intensity-dependent wet-antenna model of Leijnse et al. (2008) was added. The retrieval permutations are now organised as a complete 2 x 3 x 3 factorial of the wet-dry classification (nearby links; radar-based), the wet-antenna correction (constant; intensity-dependent; frequency- and intensity-dependent) and the γ-R relation (ITU; Belgian non-linear fit; Belgian log-log fit), giving 18 retrievals per case with a systematic three-letter naming convention (Table 2 of the revised manuscript). This design allows the isolated (marginal) effect of every processing choice to be quantified (Table 6 of the revised manuscript).

(5) A new per-step evaluation. Following the reviewer's suggestion, the Results section has been restructured so that each processing step is first evaluated in isolation (Sects. 4.1-4.4): a two-dimensional sensitivity analysis of the outlier filter, a contingency-table evaluation of the wet-dry classifications, a simplified wet-antenna time-series figure, and the γ-R fitting, including a new quantification of the minimum detectable rain rate implied by the 1 dB power quantization. Only afterwards are the combined permutations compared on case-accumulated precipitation in a dedicated subsection (Sect. 4.5), followed by the Brussels case study (Sect. 4.6).

(6) A new evaluation-metrics subsection. On request of Reviewer 2, Sect. 3.6 of the revised manuscript now defines the mean bias (with sign convention: estimate minus reference), the relative bias, the RMSE, the Pearson correlation coefficient r, the coefficient of determination R^2 (computed with respect to the 1:1 line) and the Kling-Gupta efficiency (KGE), which is adopted as the combined ranking metric, together with the matching rules and sample sizes entering each comparison.

(7) Restructured Discussion and Conclusions. The Discussion (Sect. 5) now consists of three subsections (comparison with previous nationwide retrievals; assumptions and limitations; implications for operational rainfall products), while the listing of the main findings has been moved to the Conclusions (Sect. 6).

General comments

Paper organization

Comment 1.1. *I suggest moving lines 89-92 into a new subsection within the Methods section (e.g., entitled "CML Data Reduction"), as they describe a key step in raw CML data processing rather than a marginal detail. The same applies to lines 99-105. Additionally, an important assumption underlying Equations (1) and (2) is that the measurement represents an equivalent path-averaged rainfall intensity. Assumptions behind the proposed formulas and models should be clearly and explicitly stated.*

Response: We agree. A new subsection "CML Initial Data Processing" (Sect. 3.1) has been added at the start of the Methods section. It gathers all raw data-reduction steps previously scattered previously through Sect. 2: the reported minimum and maximum signal levels, the ITU-T G.826 quality indicators used to discard erroneous records, the construction of the two attenuation extremes within a 15min window under automatic transmit power control, the decomposition of the total signal loss into its constituents, and the min-max weighting of the retrieved rain rates. The path-averaging assumption is now stated explicitly directly below the attenuation-rainfall equation.

Changes to the manuscript: New Sect. 3.1; added sentence below Eq. (3): *"An important underlying assumption of Equations (2) and (3) is that the measurement represents an equivalent path-averaged rain intensity."*

Comment 1.2. *I suggest moving Figure 4 and Tables 4 and 5 to the end of the Results section, within a dedicated subsection. Since the authors apply different methods at each stage of CML processing, it would be clearer to first present the impact of these methods on the output of each individual step, without necessarily referring to accumulated precipitation as a performance indicator. For instance: 1) outlier identification could be evaluated showing the percentage of outliers as a function of the Z-threshold, 2) wet-dry classification yields a binary outcome and is best assessed using a contingency matrix or other suitable performance metrics for binary classification, 3) The effect of different WAA compensation methods can be efficiently illustrated with an example of time series, as done in Figure 6 (which should be simplified to show only one representative time series), 4) the effect of the conversion from attenuation into rainfall intensity is presented in Figure 3, which is a result in my view, hence it can be moved to the Results section. Finally, in a dedicated subsection, the authors should examine the impact of different combinations of methods on a rainfall product, such as the accumulated precipitation during each event.*

Response: We are grateful for this suggestion, which we have adopted in full. The Results section now opens with a per-step evaluation: (i) the fraction of 15-min link samples removed by the outlier filter as a function of the Z-threshold and of the target spatial correlation, together with the sensitivity of the retrieval skill (KGE) to both parameters (Sect. 4.1, new Fig. 2); (ii) a contingency-table evaluation of the wet-dry classifications against gauge-observed wet and dry states, reporting POD, FAR, CSI, PC and HSS per case and for all cases combined (Sect. 4.2, new Table 3); (iii) a simplified wet-antenna time-series figure for a single representative event, showing the TRSL with the retrieved baseline, the wet-antenna attenuation of all three methods, and the resulting rain rates in separate panels (Sect. 4.3, new Fig. 3, replacing former Fig. 6); and (iv) the γ-R relations (former Fig. 3), which have been moved to the Results section as requested (Sect. 4.4, Fig. 4) and extended with a comparison of two fitting strategies and a new analysis of the minimum detectable rain rate (Fig. 5). The combined effect of all method permutations on event-accumulated precipitation is presented afterwards in a dedicated subsection (Sect. 4.5), where we discuss the former accumulation map figure (Fig. 6) and where the evaluation tables have been replaced by a ranking table of the best permutations (Table 5), including performance metrics, and a table of the marginal effect of each processing choice (Table 6).

Changes to the manuscript: Results restructured as Sects. 4.1-4.6; new Fig. 2, Table 3, Fig. 3 and Fig. 5; former Fig. 3 moved to Sect. 4.4; former Fig. 4 and Tables 4-5 reorganised into Fig. 6 and Tables 5-6 in Sect. 4.5.

Comment 1.3. *As pointed out by the authors (Table 4 and lines 338-339), the four events have different characteristics. I think it would be good to produce a new figure similar to Figure 4 for case 3 or 4. Please also consider merging Tables 4 and 5 into one, retaining only the column in Table 4 relative to rain gauges. The remaining columns of Table 4 are already reflected in Table 5 through bias or RMSE with respect to rain gauges.*

Response: Map figures analogous to the former Fig. 6 are now provided for Cases 2, 3 and 4 in the supplementary material (Figs. 10,11,12), and their qualitative behaviour is discussed in Sect. 4.5, including the strong radar overestimation in Case 2 and the general CML underestimation in Case 4. Regarding the two tables, we have followed the spirit of the suggestion and removed the redundancy in a slightly different way: the spatial statistics of the gridded products (former Table 4) were already embedded directly in the panels of the map figure (Fig. 6 lists the spatial mean, 99th percentile, standard deviation and autocorrelation length in each panel), and hence this table has been removed, whereas the evaluation with respect to the gauges (former Table 5) has been replaced by a ranking table of the five best permutations per case and for all cases combined, compared against RAD-QPE (Table 5), including all formerly included performance metrics and the Kling-Gupta Efficiency. The complete ranking of all 18 permutations is added in the supplement (Table 10). The two types of information (spatial variability of the gridded fields versus point evaluation at the gauges) are thereby retained without duplicating any numbers.

Changes to the manuscript: New supplementary Figs. S1-S3; former Tables 4 and 5 replaced by the panel statistics of Fig. 6 and by Tables 5, 6 and S1.

Comment 1.4. *Part of the content of Section 5 (Discussion) would be more appropriately placed in the Conclusions section. In its current form, Section 5 primarily enumerates the main findings of the analysis and emphasizes the importance of careful data processing, which is more typical of a conclusions section. A discussion section should instead focus on revisiting the underlying assumptions and limitations of the proposed approach, as well as considering alternative methodologies. In addition, the authors could use this section to present supplementary analyses (e.g., a sensitivity analysis) and to compare their results with those reported in similar studies. I recommend revising* *and rebalancing the final two sections accordingly.*

Response: We have restructured the final two sections along these lines. The listing of the main findings has been moved to the Conclusions (Sect. 6). The Discussion (Sect. 5) now consists of three subsections: Sect. 5.1 compares our results with previous nationwide CML studies in Europe (the Netherlands, Germany, Italy and the German-Czech border) and explains why our conclusions on the γ-R relation differ from those of Van van Leth et al. (2018) and Overeem et al. (2016a); Sect. 5.2 revisits the assumptions and limitations of the approach (the 1 dB quantization and 15-min MINMAX format, the ATPC impact, the transferability of wet-antenna coefficients with locally calibrated alternatives following Valtr et al. (2019) and Pu et al. (2020), the midpoint-as-point assumption, the matching radii and the limited event sample); and Sect. 5.3 discusses the implications for operational rainfall products. The sensitivity analyses themselves (outlier-filter parameters, fitting function and regression direction of the γ-R relation and the matching radius) are presented in the Results and summarised in Sect. 5.2.

Changes to the manuscript: Sects. 5 and 6 rewritten and restructured into Sects. 5.1-5.3 and 6.

Datasets

Comment 1.5. *Although the analysis is based on only a few case studies, the study is conducted at the country scale and therefore relies on a large volume of data collected from multiple sensor networks. This raises an important point: measurements from different sensors of the same type (e.g., disdrometers), or from different networks of the same sensor type (e.g., rain gauges), are implicitly treated as comparable in terms of accuracy and reliability. However, this assumption may not necessarily hold and should be explicitly addressed.*

Response: This comment proved very useful. Prompted by it, we performed an additional quality assessment of the three disdrometers and found that the instrument at Uccle exhibited anomalous behaviour: over half of its velocity-diameter matrix values fell outside the envelope expected from the Gunn-Kinzer relation (see also Figure 9), and the responsible RMI staff members confirmed that the instrument likely requires recalibration. We therefore excluded it and refitted the power laws on the two remaining disdrometers, now in the retrieval (R–γ) direction (see overarching change 2); all results in the revised manuscript have been recomputed (see General response, point 1). The mutual consistency of the two retained instruments, which are of different brands and measuring principles, is now assessed explicitly in Sect. 4.4: the log-log fits of the Melle and Liège disdrometers agree closely at all frequencies (in the retrieval R–γ form, e.g., a = 8.05 versus 8.11 and b = 0.88 versus 0.91 at 25 GHz), and the known intensity-dependent differences between the OTT Parsivel^2 and Thies LPM designs (Angulo-Martínez et al., 2018) are discussed in relation to the choice of fitting function.

Regarding the rain gauges, Sect. 2.3 has been extended to address the homogeneity of the five networks explicitly: *"All of these are governmental meteorological or hydrological networks of professionally sited, maintained and quality-controlled gauges, operating at 5-minute temporal resolution. Although hardware specifications and outlier-handling procedures are not uniformly published across agencies, the corresponding technical documentation, including the WMO siting classification of the RMI stations (Journée et al., 2023) and the quality-control procedures of the RMI AWS (Delvaux et al., 2019; Bertrand et al., 2021) and HIC (Vereecken et al., 2007) networks, is available from the respective data providers. The same set of Belgian networks was compiled and used as a single high-quality ground reference by Journée et al. (2023), who report a sensor uncertainty complying with the WMO recommendation of below 5 % and whose quality control is based on comparison of* *neighbouring gauges and against radar; this provides a consistency check across these networks and supports their use here as a homogeneous reference."* Any minor differences in reporting accuracy between the networks are likely to be small relative to the CML retrieval uncertainty and are further reduced by the aggregation to 15 minutes and the interpolation.

Changes to the manuscript: Sect. 2.3 extended with the quality-control references and the Journée et al. (2023) consistency argument; Sect. 2.5 revised to describe the two retained disdrometers; all figures and tables recomputed.

Methods

Comment 1.6. *The authors apply different algorithms at each step of CML data processing, which is a sound approach. However, I have some concerns regarding the selection of these methods and their specific settings: In general, I would recommend using only methods and thresholds that were specifically developed for the same data format, in this case, 15-min MINMAX. For example, Schleiss and Berne developed the rolling standard-deviation method for wet-dry classification using 30-second instantaneous data. It is not guaranteed that this method will perform equally well when applied to 15-min MINMAX data..*

Response: We fully agree, and this concern has shaped one of the most substantial changes of the revision. Both methods in the original manuscript that were developed for 30-second instantaneous data have been removed: the rolling standard-deviation wet-dry classification of Schleiss and Berne (2010), whose window length and standard-deviation threshold were calibrated on high-frequency sampling and whose statistics would rest on only eight samples in a 2-hour window of 15-min data, and the time-dependent wet-antenna scheme of Schleiss et al. (2013), whose characteristic decay time of about 15 minutes coincides with the temporal resolution of our records. In their place, the physically based wet-antenna model of Leijnse et al. (2008) has been added, which depends explicitly on rain intensity and microwave frequency and involves no empirical time constants. The two retained wet-dry classifications (nearby links and radar-based) were slightly modified to the MINMAX format and to automatic transmit power control following Roversi et al. (2020), and the implied simultaneity assumption of transmitted and received signal extremes is now discussed explicitly in Sect. 3.3 and in the limitations (Sect. 5.2).

Changes to the manuscript: Rolling standard-deviation classification and Schleiss et al. (2013) wet-antenna scheme removed; Leijnse et al. (2008) model added (Sect. 3.4); permutation set redesigned (Table 2).

Comment 1.7. *The chosen thresholds are sometimes reported without justification. For instance, the Z-threshold of 2.5 in Section 3.1, as well as the 2-hour and 0.8 dB thresholds in Section 3.2, are not explained. Additionally, it is unclear which coefficients were used by the authors for WAA compensation when applying the method proposed by Pastorek et al. I suggest including a sensitivity analysis to evaluate how variations in these thresholds affect the results..*

Response: A full two-dimensional sensitivity analysis of the outlier filter has been added (Sect. 4.1, new Fig. 2). Two free parameters of the outlier removal algorithm were varied systematically (the Z-threshold from 1 to 5 and the target spatial correlation ρ^* from 0.5 to 0.9), and for every parameter combination the full retrieval was repeated for all 18 permutations and all four cases. The fraction of removed samples exceeds 10 % for the most aggressive threshold of Z = 1 and falls below about 3 % for Z $\geq$ 2.5, while the KGE against the gauges drops below 0.35 for Z $\leq$ 1.5 (indicating that valid rainfall is removed together with erroneous links), rises steeply between Z = 1.5 and 2.5 and reaches a broad plateau of about 0.40 for Z $\geq$ 3. The values adopted throughout the revised manuscript, Z = 3 and $\rho^* = 0.8$, correspond to the maximum permutation-averaged KGE (0.416) and lie on this plateau, so the results are insensitive to slight variations of both parameters. Note that the selected threshold therefore differs slightly from the value of 2.5 in the original manuscript.

The 2-hour and 0.8 dB thresholds of the rolling standard-deviation method no longer appear, since that method has been removed altogether (see our response to Comment 1.6). For the Pastorek et al. (2022) correction the coefficients are now stated explicitly in Sect. 3.4: *"We use the default values of 0.1 and 0.55 for the coefficient and exponent respectively, and an upper limit for A_waa of 14 dB."* Sects. 4.3 and 5.2 add the caveat that these coefficients were derived for links operating between roughly 24 and 38 GHz and contain no explicit frequency dependence, so that their application to an E-band-rich network is an extrapolation; locally calibrating the wet-antenna model on the dense Belgian gauge network, following Valtr et al. (2019) and Pu et al. (2020), is identified as a promising avenue for future improvement.

Changes to the manuscript: New Fig. 2 and Sect. 4.1; coefficients stated in Sect. 3.4; frequency-range caveat and locally calibrated alternatives discussed in Sects. 4.3 and 5.2.

Comment 1.8. *The comparison in Figure 5 is done averaging the radar pixels within 2.5 km from each rain gauge. A similar rule is used with CMLs. It sounds arbitrary and it should be justified. This choice appears somewhat arbitrary and should be explicitly justified.*

Response: Note that Figure 5 has been removed, since several new figures were introduced and we wanted to avoid overloading the manuscript; its message is now carried by Table 5, which reports the performance statistics of the best permutations. The averaging rule the reviewer refers to is the one used throughout the evaluation tables of that section. We agree that the original text did not justify it, and we have addressed this in the revised Sect. 4.5. We kept the averaging for the radar, but now explain why. A CML does not measure rainfall at a point but averages it along its path, and a radar grid point represents an area rather than a point, so neither product is a point measurement to begin with. By averaging both over the same area, neither is favoured by the way it was sampled, and the difference between them reflects the retrieval rather than the sampling. This does mean that two areal averages are compared with a point gauge, which is unavoidable, but we consider it preferable to comparing one areal average and one linear average against a point value.

The radius itself is justified by the length of the links. We use 2.5 km, comparable to the mean link length, that is, the scale over which an individual link already averages rainfall. A much smaller radius would therefore not make the comparison more local, and would only reduce the number of gauges with a matching link. As an independent check, a separation of 2.5 km retains 97 % of the spatially structured correlation of the climatological summer variogram of van de Beek et al. (2012) at a 24 h accumulation and 98 % at 48 h, the time scales of the case accumulations; the remaining loss of correlation over this distance comes mostly from the nugget rather than from the separation itself. Averaging both products over the same area does not, however, give them the same number of samples: a 2.5 km disc contains roughly 20 to 25 radar grid points but a median of only four links, so random errors are suppressed more effectively in the radar average. No choice of radius can remove this, and we now state in Sect. 4.5 that the configuration is a compromise between keeping enough gauges in the analysis and matching the two areal products to each other as closely as possible.

To show that the conclusions do not depend on the value chosen, we repeated the full evaluation of all 18 permutations for matching radii of 1, 1.5, 2, 2.5, 3, 5 and 10 km (Review Table 9). Across this range the case-combined sample varies by a factor of six, from 126 to 773 gauge samples, yet the KGE of the best permutation stays between 0.82 and 0.87 and exceeds RAD-QPE at every radius.

Because the station set changes with the radius, the table also repeats the exercise on the 126 gauge samples that all radii have in common. There the nearest-pixel radar is by construction identical for every row (KGE = 0.73), which makes it a useful control, while the best CML permutation rises from 0.82 at 1 km and settles around 0.91 from 2.5 km onwards. Finally, we did not select the radius by optimising performance. On the common sample, agreement with the gauges improves as the radius grows, whereas pairing each gauge with only its nearest link gives 0.75. This reflects the averaging out of random retrieval error rather than a genuine gain in skill, and it yields an estimate that is progressively less local. Any criterion based on maximising a score would therefore favour the most heavily smoothed estimator, which is why we fixed the radius beforehand on physical grounds.

Changes to the manuscript: Justification of the 2.5 km radius added in Sect. 4.5, based on the mean link length with the variogram as a supporting check; explicit statement that RAD-QPE is averaged over the same radius as the CMLs, together with the reasoning and the remaining difference in sampling; nearest-pixel radar reported as a tested alternative; sensitivity across matching radii summarised in Sect. 4.5 and given in full as Review Table 9 in this response; gauges entering the evaluation now highlighted in Fig. 1.

Comment 1.9. *It's important to understand whether all the 2800 CMLs are equally reliable and contribute equally informative data. I suggest the authors address the following points: Malfunctioning CMLs should be discarded all the way, not only because they record anomalous rainfall values with respect to neighbors, but also because they exhibit anomalous or irregular patterns during dry periods. While the authors mention that some CMLs were discarded, they do not provide details on the criteria or procedure used. They only describe how outliers were identified. I recommend that the authors detail how malfunctioning CMLs were identified and removed.*

Response: We agree that this information was insufficiently documented. The new Sect. 3.1 now details the first level of screening, based on the standard ITU-T G.826 performance indicators reported by the network management system: background block errors, errored seconds, severely errored seconds and unavailable seconds, each of which is now defined in the text. Any 15-minute record with a non-zero value for any of these indicators is discarded (approximately 0.5 % of the complete dataset). The second level is the redesigned outlier filter (Sect. 3.2), which operates on the 24-hour rolling-mean retrieval. Importantly, the filter compares each link only with truly independent neighbours (links sharing no antenna with the link under test or with one another), because faults at shared antenna hubs can affect many co-located links simultaneously; a link is only evaluated when at least three independent neighbours with valid data are available. At the adopted settings the filter removes a further 2-3 % of the samples. Both fractions are now reported in the manuscript.

Changes to the manuscript: New Sects. 3.1 and 3.2 with explicit criteria, definitions of the quality indicators and the removed fractions per criterion.

Comment 1.10. *CMLs exhibit markedly different sensitivity to rainfall depending on their frequency-length combination. In my view, including a figure illustrating CML sensitivity-such as the minimum measurable rainfall intensity for different CML types-is essential.*

Response: We agree, and have addressed this suggestion with two complementary new figures: one showing the theoretical sensitivity implied by the data format, and one showing how that sensitivity translates into actual retrieval skill across the frequency–length space of the network.

The first (Sect. 4.4, new Fig. 5) shows the minimum detectable rain rate implied by the 1 dB power quantization, computed for each individual sublink as $R_{\text{min}} = (\Delta A_q/(\text{a}'L))^{1/\text{b}'}$ with $\Delta A_q = 1$ dB, L the path length and a′, b′ the attenuation-form coefficients ($\text{a}' = \text{a}^{-1/\text{b}}$) matching the frequency and polarization of the sublink. Results are grouped in three frequency bands and shown for the ITU relation and for both locally fitted relations, with the median and interquartile range per band and the number of sublinks indicated. Despite their short paths, the E-band links emerge as the most sensitive part of the network, with a median R_{min} of about 1.1 mm h^{-1} for the log–log relation, against about 2.6 mm h^{-1} at 25–45 GHz and 3.3 mm h^{-1} at 5–25 GHz; for half of the links below 45 GHz the detection limit exceeds 2.5 mm h^{-1}.

The second (Sect. 4.5, new Fig. 7) makes the same point empirically rather than theoretically. It resolves the per-link agreement with the rain gauges on a grid of link frequency against path length, showing the number of links, the bias, the RMSE and the KGE in every frequency–length cell, for the ITU relation and the locally fitted log–log relation side by side on shared colour scales. The result confirms and refines the picture of Fig. 5: the short, high-frequency links carry the highest skill and the smallest bias, whereas the low-frequency and longest links show large positive biases and low KGE, consistent with a substantial fraction of the rainfall falling below their detection limit. The grid also shows where the local calibration matters: it improves the retrieval most clearly in the short, high-frequency cells that contain the majority of the links, while the ITU relation retains a slight advantage in a few sparsely populated cells at the low frequencies and longest paths.

Both figures are cross-referenced wherever detection limits matter for the interpretation: in the wet-antenna discussion (Sect. 4.3), the permutation evaluation (Sect. 4.5), the Brussels case study (Sect. 4.6), the limitations (Sect. 5.1) and the Conclusions.

Changes to the manuscript: New Fig. 5 and accompanying text in Sect. 4.4; new Fig. 7 and accompanying text in Sect. 4.5; cross-references throughout Sects. 4–6.

Comment 1.11. *Moreover, assessing CML performance across subsets of CMLs would be highly informative. The authors present an analysis dividing the CMLs in three frequency bands in Figure 7 of Section 4.4, which is briefly commented. Case 2 shows problematic performance, with numbers in Table 5 worsening when using RID, likely due to the relatively low accumulated rainfall (as seen in Figure 7). It would be valuable to explore whether focusing on the most sensitive CMLs can reduce this large bias. Additionally, the authors could provide a "rule of thumb" on CML accuracy under different rainfall conditions, which would help interpretation of CML-based rainfall estimates. Finally, apart from outliers, it's also interesting to investigate whether there are CMls constantly under/overestimating rainfall.*

Response: Several additions address this comment. First, the frequency-based evaluation has been substantially expanded and redesigned (Sect. 4.5, Fig. 7). Rather than three frequency bands, the revised figure resolves the per-link agreement with the gauges jointly on a frequency × length matrix, for the ITU relation (RFI) and the local log–log relation (RFL) side by side, showing the number of links, the bias, the RMSE and the KGE in every frequency–length bin. It shows that the benefit of the local calibration is concentrated in the short, high-frequency cells (paths below 2 km at 20–90 GHz) and the mid-frequency cells, where RFL improves the KGE over RFI and brings the bias close to zero, while ITU retains a slight advantage only for the longer high-frequency links and the low-frequency links; the count panels confirm that the cells favouring the local relation contain the large majority of the links. This provides the requested rule of thumb, which is now stated in the text: the low-frequency and longest links are limited by their detection threshold and benefit least, whereas the short, high-frequency links that dominate urban subnetworks carry the highest skill and benefit most from local calibration. The revised text draws the practical conclusion that *"operational rainfall products may benefit from down-weighting or excluding the low-frequency links during light and moderate rainfall events."*

Second, regarding the most sensitive links and Case 2: the concern raised for the original Table 5 is largely resolved by the revised processing itself. With the refitted relations and the redesigned permutations, the best CML retrievals for Case 2 are nearly unbiased at the country scale (relative biases of about 5-16 % for the leading permutations), whereas RAD-QPE overestimates the sparse showery rainfall of this case by a large margin (Table 5), possibly related to hail. In addition, the evaluation over the Brussels-Capital Region (Sect. 4.6), where 70 % of the links are E-band and hence the most sensitive subset of the network (Fig. 5), effectively constitutes the restriction to sensitive links suggested by the reviewer: there, the CML retrievals clearly outperform RAD-QPE for Case 2 as well (Table 8).

Third, regarding links that consistently over- or underestimate: we investigated this, but with only four events (two of which produced very little rainfall over large parts of the network) we found that a per-link bias consistency analysis cannot be separated robustly from the sampling variability of scattered convection, and we prefer not to include a statistically fragile result. The limitations section now notes that longer records, rather than additional analyses of the same events, are required for such link-level characterisation (Sect. 5.2). We hope the reviewer agrees that this is best left to a follow-up study based on a longer data record.

Changes to the manuscript: Expanded Fig. 7 and accompanying rule-of-thumb text in Sect. 4.5; Case 2 discussion in Sects. 4.5 and 4.6; limitation noted in Sect. 5.2.

Introduction

Comment 1.12. *I think it should be completed with some important information: Lines 28 on (limitations of CMLs): an important limitation of several CML datasets is the non-optimum format for rainfall estimation. In particular, the 1 dB signal quantization is a limitation in the presence of light rainfall. In addition, the 15-min MINMAX format is not ideal. And by way, this is the format of the CML dataset available in this work. Please mention these issues + references.*

Response: Agreed. The Introduction now explicitly identifies the data format as a limitation among the CML error sources, and, more importantly, the revised manuscript treats this limitation quantitatively rather than only qualitatively: the new minimum-detectable-rain-rate analysis (Fig. 5, see our response to Comment 1.10) makes the consequence of the 1 dB quantization explicit for every link in the network, and the Discussion opens its limitations subsection with the statement that *"the most fundamental limitation of this study is the data format rather than any individual processing step"*, followed by its three consequences (a hard detection limit; a baseline and wet-antenna uncertainty of the same order as the quantization step during light rain; and the ATPC simultaneity assumption of the transmitted/received signal extremes), with the note that these would be relaxed by 1-min instantaneous sampling as used by Graf et al. (2020). In the Introduction we have added: *"A further limitation of many operational CML datasets, including the one used here, is the data format itself: signal levels are typically quantized at 1 dB and stored as 15-minute minima and maxima, which restricts the detectability of light rainfall (Overeem et al., 2016a; Chwala and Kunstmann, 2019)."*

Changes to the manuscript: Sentence and references added to the Introduction; new Fig. 5 (Sect. 4.4); Discussion Sect. 5.2, first paragraph.

Comment 1.13. *Since this is a country-wide study, the authors should include a paragraph summa-*

rizing previous research that used nationwide CML networks. They should highlight how this study differs from earlier work, for example in terms of climatic region, rainfall characteristics, sensor types, network density, or data processing approaches. This comparison will help contextualize the novelty and contribution of this study.

Response: Such a paragraph has been added to the Introduction: *"Nationwide CML rainfall retrieval has so far been demonstrated in only a handful of European countries, most notably in the Netherlands (Overeem et al., 2013, 2016b), Germany (Graf et al., 2020), Italy (Roversi et al., 2020), and across the German-Czech border (Blettner et al., 2023). These studies generally considered relatively homogeneous networks operating at low to mid-range microwave frequencies (typically below 40 GHz), with few or no E-band links. In contrast, the Belgian network analysed here spans a much broader frequency range (7-85 GHz), including a substantial proportion of short E-band links. Furthermore, whereas previous nationwide studies have relied primarily on gauge-adjusted radar for validation, we evaluate the retrievals against both a dense operational rain gauge network and the national radar QPE, while systematically assessing the influence of the individual processing steps."* In addition, a dedicated Discussion subsection (Sect. 5.1) now compares our results in detail with these earlier nationwide studies, including the sampling strategies (15-min MINMAX versus 1-min instantaneous) and the path-length and frequency distributions.

Changes to the manuscript: New paragraph in the Introduction; new Sect. 5.1.

Comment 1.14. *Line 43: The term "non-uniform beam-filling" may be somewhat misleading in this context. In radar meteorology, it refers to the fact that an elemental radar resolution volume ("radar cell") may not be fully filled with precipitation, particularly at long range where the cell's angular size can exceed 1 km while its radial size is typically around 100 m. For CMLs, this concept does not directly apply because: 1) a CML antenna beam is much narrower than the one of weather radars over practical CML ranges and 2) The received signal loss results from attenuation along the entire propagation path, whereas radar measures backscatter only from particles within the radar cell (and any path attenuation is considered a disturbance). In other words, the "beam" for CMLs corresponds to the full electromagnetic path between transmitter and receiver, while for pulse radars it refers only to the portion of the beam illuminating a specific radar cell.*

Response: We thank the reviewer for this clarification and agree. The term has been removed and the sentence rephrased in terms of the path-integrated nature of the CML measurement: *"They are also less affected by beam broadening because the propagation paths are typically only a few hundred metres to several kilometres long (Berne and Uijlenhoet, 2007). For longer links, however, rainfall variability along the propagation path, combined with the non-linearity of the attenuation-rainfall relation, degrades retrieval accuracy; this is particularly relevant in tropical regions, where long (10-25 km), low-frequency (<10 GHz) links are common."*

Section 2

Comment 1.15. *Table 1, caption: the last statement is unclear and appears unnecessary..*

Response: The sentence has been removed from the caption of Table 1.

Comment 1.16. *Line 81: the authors did not state what they mean by "sublink".*

Response: A definition has been added at first use in Sect. 2.2: *"over 1600 CMLs (comprising about 2800 sublinks, denoting one directed transmission channel of a link; each physical CML path typically comprises two sublinks operating in opposite directions)".*

Comment 1.17. *Line 99: the statement is unclear: the authors are stating that "specific attenuation" (dB/km) and "path-average attenuation" (dB) are the same thing.*

Response: Corrected. In the new Sect. 3.1 the specific attenuation γ (dB/km) is introduced unambiguously through the division of the attenuation terms by the path length in Eq. (2), and the conflicting wording has been removed.

Comment 1.18. *Lines 113-114: The term "independent data points" is unclear. It should be clarified in the context of the specific analysis being performed. For example, measurements taken at similar frequencies along the same CML path are highly correlated and cannot be considered independent. The authors should explain how they define independence and justify its use in the analysis.*

Response: We agree that the wording was ambiguous. What was meant is that both sublinks of each link are carried through the retrieval and the interpolation as separate samples; it was not meant to imply that the two sublinks of a path are statistically independent, which they are indeed not. The sentence has been rephrased in the revised manuscript as: *"Both sublinks of each link are retained as separate samples, although sublinks sharing a path are not independent."* We note that where statistical independence actually matters in the analysis, namely in the outlier filter, dependence between links is actually handled explicitly: only links that share no antenna with the link under test or with one another are admitted as neighbours (Sect. 3.2).

Comment 1.19. *Sec 2.3: rain gauge data. Since these data serve as the ground truth for validating CML results and are collected from multiple networks, some basic considerations regarding their homogeneity are due. For example: Is the measurement resolution (e.g., 0.2 mm) consistent across all networks, or does it vary? Do all networks follow similar procedures for data quality control? These points are important to determine whether the rain gauge data can be considered equally reliable across networks. Additionally, Figure 1 shows that sensors from different networks are sometimes located very close together. It may be useful to compare their daily accumulation values or reference previous studies that have assessed inter-network consistency, to support the assumption of data reliability.*

Response: We thank the reviewer for this point, which is closely related to Comment 1.5. Sect. 2.3 has been extended as quoted in our response to that comment: the five networks (RMI, VMM, HIC, SPW Mobilité et Infrastructures, and IBGE) are all operated by governmental meteorological or hydrological services, and the available technical documentation on siting and quality control is now referenced (Journée et al., 2023; Delvaux et al., 2019; Bertrand et al., 2021; Vereecken et al., 2007). Importantly, this exact combination of Belgian networks was compiled and used as a single high-quality ground reference by Journée et al. (2023), whose quality control is based on comparison of neighbouring gauges and on comparison against radar, and who report a sensor uncertainty complying with the WMO recommendation of below 5 %. This constitutes a published, operational assessment of inter-network consistency across precisely these networks, and we now reference it to support the assumption of cross-network reliability.

Regarding the suggestion to intercompare closely spaced gauges from different networks: we would prefer not to add such an analysis, for two reasons. First, truly co-located cross-network pairs are few, and the scatter between neighbouring gauges is dominated by genuine sub-kilometre rainfall variability, particularly for the convective events studied here, so the comparison would be statistically underpowered as a homogeneity test and would duplicate the neighbour-based quality control already performed operationally by Journée et al. (2023). Second, the gauge networks serve here as an established reference whose inter-network differences are second-order compared with the CML uncertainties that are the focus of the paper. We have instead made the origin and quality control of the reference data explicit in the text, and we hope the reviewer finds this an acceptable resolution.

Changes to the manuscript: Sect. 2.3 extended with the network descriptions, quality-control references and the Journée et al. (2023) consistency argument.

Comment 1.20. *Line 151: hydrometeor instead of hydrometer. Figure 3: mm/h is used here, while mm/hr is used somewhere else in the manuscript. Please use consistent abbreviations.*

Response: Both corrected; mm h^{-1} is now used consistently throughout the revised manuscript, including all figures and tables.

Section 3

Comment 1.21. *The topic of CML-based rainfall estimation has been studied for some time, and the fundamental steps of data processing are well established. While the authors have selected and tested a few methods on their dataset, many alternative approaches have also been proposed. For the sake of completeness, the manuscript should acknowledge these alternatives or refer to relevant review papers on CML processing methods. For example, only three IEEE journal papers are currently cited, whereas numerous other studies-particularly focusing on CML signal processing-have been published and are pertinent.*

Response: The literature basis of the revised manuscript has been broadened considerably. The review of Chwala and Kunstmann (2019) is cited as the entry point to the breadth of processing approaches, and the individual method sections now acknowledge the main alternatives: for the wet-dry classification, rolling standard-deviation methods (Schleiss and Berne, 2010; Graf et al., 2024), nearby-link methods (Overeem et al., 2016a), and auxiliary radar (Overeem et al., 2011) or satellite information (van het Schip et al., 2017); for the wet-antenna correction, the constant, time-dependent, intensity-dependent and physically based formulations, complemented in the Discussion by locally calibrated approaches from the signal-processing literature suggested by the reviewer (Valtr et al., 2019; Pu et al., 2020). The new Sect. 5.1 further engages with the nationwide processing studies of Overeem et al. (2013, 2016b), Graf et al. (2020), Roversi et al. (2020) and Blettner et al. (2023), and the disdrometer processing now references the dedicated instrument-comparison literature (Angulo-Martínez et al., 2018) and the DISDRODB framework (Ghiggi et al., 2026).

Changes to the manuscript: References added throughout Sects. 1, 3, 4.4, 5.1 and 5.2.

Comment 1.22. *Line 160: The terminology is unclear. By "seconds," do the authors mean individual samples? This should be clarified, as the raw CML data are not recorded at one-second intervals. Similarly, the term "background block error" is not defined.*

Response: Clarified in the new Sect. 3.1. The quantities are the standard ITU-T G.826 performance indicators reported by the network management system, and each is now defined at first use: *"background block errors (BBE; errored transmission blocks outside severely errored periods), errored seconds (ES; one-second intervals containing at least one transmission error), severely errored seconds (SES; one-second intervals with severe transmission degradation), and unavailable seconds (UAS; one-second intervals during which the link is classified as unavailable). These are provided as cumulative values by the network management system for each 15-minute interval and used as a first quality flag."*

Comment 1.23. *Lines 174-180: The rationale for outlier filtering is unclear. Initially, neighbors are described as being determined based on a long-term (30-year) estimate of spatial rainfall correlation (lines 174-176). However, in the following sentence, the authors state that neighboring CMLs are defined differently: "All CMLs within a circular distance of the CML in question, where the spatial correlation for that date exceeds 0.6, are considered neighboring CMLs." It is therefore unclear which definition of neighboring CMLs is actually used in Equation (3).*

Response: This was indeed poorly worded, and the entire outlier-filter description has been rewritten and formalised (Sect. 3.2). A single definition is now given: neighbouring links are all links whose midpoints lie within a search radius r of the link under test and that share no antenna with it or with one another. The radius r is the distance at which the climatological spatial correlation of 24-h rainfall for the relevant day of year, derived from the 30-year spherical variogram of van de van de Beek et al. (2012) (now given explicitly as Eqs. 5-6), drops to a target value ρ^*. No event-specific correlation is involved; because the climatological variogram varies seasonally, the radius adapts automatically to the expected decorrelation length of the time of year. The target correlation $\rho^* = 0.8$ and the Z-threshold are selected through the sensitivity analysis described in our response to Comment 1.7.

Changes to the manuscript: Sect. 3.2 rewritten with Eqs. (5)-(7) and the unambiguous neighbour definition.

Comment 1.24. *Section 3.1: A straightforward way to assess the effectiveness of outlier filtering is to compare the number of samples removed by SCI relative to SCI-U. This number likely depends on the chosen Z-threshold. Currently, there is only a brief mention of outliers later in the manuscript (line 299). I recommend that the authors analyze and report how the percentage of removed outliers varies with different Z values, as this would provide important insight into the sensitivity and robustness of the outlier filtering step.*

Response: This analysis has been added (Fig. 2a); see also our response to Comment 1.7. The fraction of removed 15-min samples exceeds 10 % at Z = 1, decreases rapidly with increasing Z and falls below about 3 % for Z $\geq$ 2.5, with only a weak dependence on the target correlation. At the adopted settings (Z = 3, $\rho^* = 0.8$), 2-3 % of the samples are removed, which is substantially more than the fraction of records discarded through the errored-seconds quality flags (about 0.5 %). The effect of the filter on the retrieved fields is retained in the permutation comparison through the unfiltered -U variant (Fig. 6c versus d).

Comment 1.25. *Section 3.2, last statement: It is unclear how the three 5-min radar samples were combined. Did the authors simply average them and then apply the 0.1 mm/h threshold? Another valid approach would be to take the maximum of the three time slots, since CML data are MINMAX and, in principle, can capture any rainfall occurrence within each 15-min interval (subject to sensitivity limits due to quantization).*

Response: The three 5-minute accumulations are summed to a 15-minute accumulation, and a CML record is classified as wet if at least one RAD-QPE pixel along the CML path indicates more than 0.15 mm of rain within that 15-minute interval. Note that we tried values of 0.05 to 0.2 mm per 15 minutes, and the 0.15 mm value proved optimal, although the sensitivity to this exact value was limited. This is now stated explicitly in Sect. 3.3. We agree that a maximum-based criterion is a natural alternative for MINMAX data. We note, however, that with such a low absolute threshold the summed criterion behaves very similarly to a maximum-based one in practice: any single 5-minute slot contributing some rain along the path likely already triggers the wet classification.

Furthermore, the number of samples to assess the maximum from the radar would only be three, while for the CML network management system this is likely to be much higher. The detection behaviour of the resulting classification is now assessed objectively against the gauges in the new contingency analysis (Table 3), where its conservative character (fewer false alarms, more misses of light rain near the detection limit) is quantified and discussed.

Comment 1.26. *Section 3.3, regarding the Pastorek method for WAA compensation: It is unclear whether the authors used the same power-law coefficients as in Pastorek et al. Those coefficients were derived from CMLs operating in the 24-38 GHz range, which may differ from the frequencies of the links in this study. This point is important and should be explicitly clarified in the manuscript. While calibrating the WAA coefficients using local rain gauge data could improve the results, I understand that this is a substantial task. The authors appropriately note it as future work in the discussion. However, I think the authors can elaborate more on this item (maybe in the discussion section), as there are several WAA compensation methods based on local data and the authors have a very dense rain gauge network available. See, for instance: Valtr et al., 2019, 10.1109/LAWP.2019.2925455; Pu et al.,2020, 10.1109/LAWP.2020.3011463.*

Response: Both suggestions have been implemented; see also our response to Comment 1.7. The coefficients are now stated explicitly in Sect. 3.4 (0.1 and 0.55, with an upper limit of 14 dB), and both Sect. 4.3 and Sect. 5.2 make the calibration range explicit: the Pastorek et al. (2022) relation was derived for links operating between roughly 24 and 38 GHz and contains no explicit frequency dependence, so its application to an E-band-rich network involves an extrapolation, which the revised marginal-effect analysis identifies as a likely contributor to the systematic positive bias of these permutations (Table 6). The Discussion elaborates on locally calibrated wet-antenna approaches as suggested: *"A more satisfactory solution would be to calibrate the wet-antenna model on local data, as done by Valtr et al. (2019) and Pu et al. (2020), and the dense Belgian gauge network would in principle allow this. We did not attempt it here, since a robust calibration requires a much longer record than four events and would need to be stratified by frequency and antenna type, but it is a promising avenue for improving the retrievals."*

Comment 1.27. *Line 255: minimum or maximum deviation?*

Response: This criterion has been superseded: the quality control of the disdrometer spectra was overhauled during the revision and now follows the standardized DISDRODB procedures (Sect. 3.5): *"drop counts are discarded when the measured fall velocity deviates by more than 50 % from the terminal velocity of rain drops following Beard (1976). Small drops (D < 1 mm, v < 2.5 m s^{-1}) are exempted from this criterion, as turbulence may legitimately displace them from their terminal velocity, and drop counts associated with splashing on the instrument (v $\leq$ 0.6 m s^{-1} in time steps flagged as splashing-affected) are removed."* The ambiguous minimum-deviation wording no longer appears.

Comment 1.28. *Line 274: Add a reference that reports the DSD variability between maritime and continental environments*

Response: A reference has been added to the corresponding statement in Sect. 4.4 (Bringi et al., 2003), which documents the systematic differences in drop size distributions between maritime and continental rainfall regimes.

Comment 1.29. *Lines 285-286: it's the same method already referred to in Sec.2.3. Maybe a shorter statement is better "... with the same kriging method used for rain gauge data (see Sec.*

3.1)"

Response: Rephrased as suggested; the Results now simply refer to *"the ordinary kriging procedure of Sect. 2.3"* wherever the interpolation is mentioned.

Comment 1.30. *Figure 4a: The radar product shows a few linear stripes oriented SSW to NNW with one particularly evident in central Belgium. Are they artifacts rather than true rainfall structures?*

Response: These are true rainfall structures related to the advection of intense, localised showers from SSW to NNE, and later from SSE to NNW, as the winds were shifting throughout the day. The same elongated accumulation bands are also present to a lesser extent in the interpolated gauges and the CML retrievals (Fig. 6), which supports their meteorological origin.

Section 4

Comment 1.31. *Table 5 presents important results that deserve further investigation. I would expect SCI results to outperform SCI-U. However, in Cases 1 and 4, both bias and relative bias are clearly worse with SCI. In Case 2, the very high relative bias for CMLs is likely due to low accumulated rainfall measured by the gauges combined with the 1-dB quantization, which limits CML sensitivity. I am pretty sure that the results would improve if the analysis were restricted to the subset of CMLs with higher sensitivity, Can the authors elaborate more on these points?*

Response: The rolling standard-deviation classification has been removed from the revision (General response, point 4), so the comparison the reviewer refers to is now between NCI-U and NCI, that is, the same permutation with and without outlier filtering. The behaviour noted is now explained by the outlier-filter sensitivity analysis (Sect. 4.1, Fig. 2), which makes explicit that filtering involves a trade-off: aggressive settings remove genuine convective peaks together with the artefacts, so that the filter cannot be justified by its effect on the bias alone. The KGE, which penalises errors in bias, variability and correlation simultaneously, exposes this trade-off directly: it degrades quickly for aggressive thresholds, rises steeply as the threshold is relaxed, and plateaus for $Z \geq 3$. The filter is therefore justified on this plateau, where it removes the isolated bull's-eye artefacts and the excessive extremes (Fig. 6c versus d) while leaving the bulk of the rainfall untouched.

Regarding Case 2 and the sensitivity of the links, the reviewer's expectation is confirmed by the revised analysis along three lines. First, at the country scale the recomputed retrievals (with the refitted R–γ relations and the redesigned permutation set) are close to unbiased for Case 2, with relative biases of the leading permutations ranging from near zero to about 16 %, whereas RAD-QPE overestimates this case considerably, possibly related to the large hail reported during the event (Table 5). Second, the stratification the reviewer proposes is now possible directly: the new frequency–length skill grid (Fig. 7) reports the bias, the RMSE and the KGE of every frequency–length cell separately, so that the performance of any subset of links with a given sensitivity can be read from it. It confirms that skill is not uniform across the network but concentrated in the short, high-frequency links, which have the lowest detection limits (Fig. 5), while the cells combining the lowest frequencies with the longest paths show the weakest agreement with the gauges. Third, an evaluation effectively restricted to the most sensitive part of the network is provided by the Brussels-Capital Region analysis, where 70 % of the links are E-band with a median detection limit of about 1.1 $\mathrm{mm\,h^{-1}}$: there the CML retrievals for Case 2 clearly outperform RAD-QPE at 15-min resolution (Table 8). The link between sensitivity and skill is thus traceable throughout the manuscript, from the detection-limit analysis (Fig. 5) through the frequency–length evaluation (Fig. 7) to the urban case study; see also our response to Comment 1.11.

Changes to the manuscript: Sects. 4.1, 4.4, 4.5 and 4.6; Figs. 2, 5 and 7; Tables 5 and 8.

Comment 1.32. *Figure 5: Averaging radar pixels within 2.5 km of each rain gauge may not be entirely justified unless there is a clear physical reason (e.g. advection of rain cells). One of the main advantages of radar is its high spatial coverage, and in fact each rain gauge falls within a radar pixel. A different approach could be to use the radar pixel containing the rain gauge or, alternatively, a bilinear interpolation of the four surrounding pixels.*

Response: We agree that the nearest pixel is the natural choice when radar is evaluated on its own, and our reason for averaging is not physical but comparative. The difficulty is that the three products represent rainfall at three different scales. The gauge is a point, the radar pixel is an area of about 1 km^2, and a CML integrates along a path of several kilometres. Only for the radar does a value exist at the gauge location; no CML is ever co-located with a gauge, so the CML estimate must in some way be aggregated over the links in the vicinity. If we then took the nearest radar pixel, we would be comparing a point measurement with a linear average and with a single grid cell, each at a different scale. By averaging both the radar and the CMLs over the same disc, at least these two are brought to a common scale before being compared with the gauge. The comparison with a point measurement remains imperfect for both, but it is imperfect in the same way, which is what allows the difference between them to be attributed to the retrieval rather than to the sampling.

The same reasoning is why we do not pair each gauge with its single nearest link. That would reintroduce the scale mismatch we are trying to avoid, and it would also require an arbitrary decision on how far a link may be from the gauge before the pair is discarded, with no obvious value to choose. The last row of Table 9 shows what happens if one does this: pairing each gauge with its nearest link within 5 km, the best permutation reaches a KGE of 0.75 against 0.91 for the 2.5 km average on the same gauges. Much of the agreement with the gauges evidently comes from averaging several links, which is expected if part of the error of an individual link is random.

We did test the alternative the reviewer proposes. Both radar samplings are in fact carried through the whole evaluation: Table 9 reports RAD-QPE both at the nearest grid point and averaged over the same radius as the CMLs. The two agree closely at the radius we use, differing by 0.003 in case-combined KGE at 2.5 km (0.653 against 0.650) and by no more than 0.03 in any single case, so the radar results do not depend on this choice. Its departure from the gauges is mostly a bias, and averaging a few neighbouring pixels does not remove a bias. The radius itself is not decisive either. On the 126 gauge samples that all pairing rules have in common, the best permutation ranges from 0.82 at 1 km to 0.91 at 2.5–3 km, while the nearest-pixel radar is by construction identical for every row at 0.73, so the CML retrievals outperform the radar benchmark at every radius. We use 2.5 km because it is comparable to the mean link length and retains most of the spatially structured correlation of summer rainfall at the accumulation times of our cases (response to Comment 1.8), while keeping enough gauges for the evaluation.

For the Brussels evaluation we use a smaller radius of 1 km, which comes close to what the reviewer suggests: at that radius the disc contains only a few grid points, so the radar average differs little from an interpolation of the surrounding pixels. Three things motivate the smaller radius there. The accumulation interval is 15 min rather than a whole case, and the variogram of van de Beek et al. (2012) decorrelates faster at shorter time scales; the Brussels links are much shorter (0.81 km on average), so each represents a smaller area; and the IBGE network is dense enough that a 1 km radius still leaves most gauges with a link.

Changes to the manuscript: Justification of the matching radius and of the identical treatment of both areal products added to Sect.4.5; radius sensitivity summarised there and in Sect. 4.6.

Comment 1.33. *Figure 5: It would be important to check whether the performance of the RAD-QPE product changes when considering only the truly independent rain gauges from the IBGE network. The authors may elaborate on the RAD-QPE performance in BCR, where IBGE and other networks are deployed, comparing RAD-QPE against rain gauges of different networks.*

Response: This evaluation is central to the revised Sect. 4.6: the entire Brussels-Capital Region assessment is performed against the IBGE network, which is fully independent of RAD-QPE since it is not used in the mean-field bias adjustment (Sect. 2.4). Against these independent gauges, RAD-QPE reaches a case-combined KGE of 0.64 with a relative bias of 20 % and an R^2 of 0.39 at 15-min resolution (Table 8), which is very similar to its skill against the (partly ingested) country-wide gauge set for the case accumulations (KGE 0.65, Table 5). This similarity indicates that the country-scale evaluation is not strongly inflated by the partial dependence between RAD-QPE and the reference gauges, a point that is reinforced by the fact that the mean-field bias adjustment operates on 5-minute domain-mean amounts and that no additional adjustment towards case totals is performed.

Changes to the manuscript: Sect. 4.6 and Table 8 (independent IBGE evaluation);

Comment 1.34. *Figure 5 caption: "The colors denote the different cases represented as shown in the legend". Are you referring to the legend of previous Figure 1b?*

Response: The former Figures 5 and 10 have been replaced by the ranking tables (Tables 5 and Table 8), and former Figure 7 has been replaced by a more complete Frequency x Length based evaluation of CML performance (Fig. 7).

Comment 1.35. *Figure 6: it should be modified as it is unclear. The subfigures should clearly show the dry periods before and after the end of the rain event (at least over a few hours), which is not the case for the links 25.4 and 81.2 GHz). In addition, I suggest showing only one example with TSRL, WAA and rain rate displayed over 3 rows. Table 5: The header for "Case 1" is missing*

Response: The former Fig. 6 has been replaced entirely (new Fig. 3). The new figure shows a single representative event (Case 1, 22 June 2023), including the dry periods before and after the rainfall, with the three requested quantities in separate panels: the TRSL with the retrieved baseline, the wet-antenna attenuation of each method, and the resulting rain rates, with grey shading marking the intervals classified as wet. We retained two links (one at 17.8 GHz and 7.5 km, one at 81.5 GHz and 0.7 km) rather than a single one, because the explicit frequency dependence of the newly added Leijnse et al. (2008) correction, which is central to the revised manuscript, can only be illustrated by contrasting a low- and a high-frequency link; we hope the reviewer agrees that this serves the purpose of the figure. The missing Case 1 header no longer applies, since the former Table 5 has been replaced by Table 5 of the revised manuscript, in which all case blocks are labelled.

Changes to the manuscript: New Fig. 3 (Sect. 4.3); former Fig. 6 and Table 5 removed.

Comment 1.36. *Reporting the outcomes of wet-dry classification outcomes is important. I would appreciate a contingency matrix or an histogram of any other performance indicator. I think that interpreting the maps in Figure 4 (final rainfall products), in terms of wet-dry classification (an initial step of CML data processing), is not entirely appropriate (lines 333-345). It can be done only for Figures 4d, e and f (NCI vs RCI vs SCI), where the difference lies in the wet/dry classification* *algorithm. By the way, these 3 figures are very similar. Moreover, as I wrote in the general comment, It would help adding a figure analogous to Figure 4 for another case and see how panels d-f look like.*

Response: A full contingency evaluation of the wet-dry classifications against gauge-observed wet and dry states has been added (Sect. 4.2, new Table 3), reporting the probability of detection, false alarm ratio, critical success index, percent correct and Heidke skill score, per case and combined over all cases. Combined over all cases, the radar-based classification is the more conservative of the two retained methods (POD 0.57 versus 0.74, FAR 0.35 versus 0.53) and achieves slightly better combined scores (CSI 0.43 versus 0.41, HSS 0.56 versus 0.50). The interpretation of the retrieved rainfall amounts in terms of the wet-dry classification is now based on these contingency metrics and on the successive-modification design of the revised map figure, in which consecutive panels alter exactly one processing step at a time (Fig. 6d versus e isolates the wet-dry classification), rather than on visual comparison of final products. Corresponding maps for Cases 2-4 are provided in the supplement (Figs. 10,11,12), as also requested in Comment 1.3.

Changes to the manuscript: New Table 3 and Sect. 4.2; map interpretation rewritten in Sect. 4.5; supplementary Figs. S1-S3.

Comment 1.37. *Lines 362-365: comment of WAA compensation. The difficulty in detecting light rainfall is primarily due to the 1 dB data quantization format.. Indeed, subtracting a WAA attenuation in the order of 2 dB or less is problematic, when the baseline itself may contain a 1 dB error. The authors should explicitly remind the reader of this fundamental data limitation when explaining the results, including in the discussion section..*

Response: Agreed, and this is now made explicit in both places. Sect. 4.4 and Sect. 5.2 now explicitly mention this: *"During light rainfall, the rain-induced attenuation, the wet-antenna attenuation and the quantization uncertainty are consequently all of comparable magnitude, so that the retrieved rain rate becomes very sensitive to the estimation of A_waa and on the accuracy of the baseline."*. Both passages refer to the new detection-limit analysis (Fig. 5).

Comment 1.38. *Lines 387-391: drawing this conclusion based on a single example is not correct in my view. The better agreement may be influenced by other factors, as a direct comparison with rain gauges over a time series depends on the relative distance between instruments, as well as on the characteristics and temporal evolution of the rainfall cell.*

Response: We agree. The conclusion in question has been removed; the systematic evidence for the effect of the locally fitted R–γ relation is now provided by the per-link skill evaluation on a frequency x length grid over all events and stations (Fig. 7) and by the Brussels ranking at 15-min resolution (Table 8), while the time-series figure (Fig. 3) is presented purely as an illustration of the mechanics of the wet-antenna corrections.

Comment 1.39. *Section 4.4: The authors should include a brief description of the characteristics of the CMLs within the BCR. For example, how many CMLs are included, and what are their mean frequency and link length?*

Response: Added in Sect. 4.6: *"BCR contains 274 links with frequency range of 22.5-81.9 GHz with 70 % in the E-band, and length range of 0.16-2.03 km."* The text also notes that the detection limits are least restrictive for these links, with a median minimum detectable rain rate of about 1 mm/h, which is what makes the evaluation at the native 15-minute resolution meaningful.

Comment 1.40. *Figures 8 and 9: The authors conclude that RID is the best CML-based output.*

Therefore, it may not be necessary to present the other outputs at this stage of the paper. Figure 9 :in my view, it does not add significant value to the paper and could be removed.

Response: We have largely followed this advice: the former Fig. 9 (the BCR time series of all permutations) has been removed. For the BCR map figure (now Fig. 8 of the revised manuscript) we retained two CML panels rather than only the best product: the retrieval with the ITU relation (RFI) and the retrieval with the locally fitted log-log relation (RFL), which are otherwise identical. Since the BCR subnetwork is dominated by E-band links, for which the effect of the local calibration is largest, this pairing visualises the impact of the R–γ relation (the ITU-based panel overestimates across the region, while the locally calibrated panel matches the gauges closely). We hope the reviewer agrees that this restricted comparison is instructive; all other permutations appear only in the ranking tables.

Changes to the manuscript: Former Fig. 9 removed; BCR map figure kept as RAD-QPE, gauges, RFI and RFL (Fig. 8).

Comment 1.41. *Table 7: It is not straightforward to compare Table 7 with Table 5, as both the CML population and the products differ (15-minute rainfall accumulation versus accumulation over an entire event). However, there is a striking difference in Case 2: the large bias observed in Table 5 is reduced to a small bias in Table 7 (RID). Could this be due to the different set of CMLs used?*

Response: Yes, largely, and this is now made explicit. The two evaluations differ in link population (the full national network within 2.5 km of the country-wide gauges, versus the E-band-dominated BCR subnetwork within 1 km of the IBGE gauges), in temporal aggregation (case totals versus 15-minute values) and in the rainfall regime sampled. The revised manuscript states these differences explicitly in Sect. 4.6, both tables now report their sample sizes and share the metric definitions of Sect. 3.6, and the mechanism behind the population dependence is traceable through the detection-limit analysis (Fig. 5) and the frequency x length skill evaluation (Fig. 7): the E-band links of the BCR are the most sensitive subset of the network, which is why the Case 2 skill is markedly better there. We also note that, with the recomputed retrievals, the large Case 2 bias of the original Table 5 no longer occurs at the country scale either (see our response to Comment 1.31).

Section 5 and Conclusions

Comment 1.42. *Lines 437-438 versus lines 433-435: It is unclear whether the dry-wet classification using radar data truly outperforms the other two methods or is only slightly better. In my view, the most appropriate way to assess this is through a contingency table. Indeed, the authors have not presented the combined cases of outlier elimination, WAA compensation via the Pastorek model, gamma-R estimation by local disdrometers, and the three wet/dry classification methods.*

Response: Both points are addressed by the revised design. The contingency table (Table 3) now provides the objective binary comparison: the radar-based classification achieves better combined scores than the nearby-link approach in all cases, mainly through its considerably lower false alarm ratio, although the differences in binary skill are indeed fairly limited. Interestingly, the factorial evaluation of all permutations reveals that the consequences for the rainfall amounts are much larger than the binary scores alone suggest (mean KGE of 0.79 for the radar-classified permutations against 0.60 for the nearby-link ones; Table 6), because the frequent false alarms of the nearby-link method convert dry-period signal fluctuations into spurious rainfall, whereas the additional misses of the radar-based method mostly concern light rainfall near or below the detection limit. This distinction between binary skill and its downstream effect is now discussed explicitly in Sects. 4.5 and 5.2. Regarding the combinations: the complete 2 x 3 x 3 factorial now covers every combination of outlier filtering, the Pastorek correction and the disdrometer-based relations with both retained wet-dry classifications (e.g., permutations RIL, RIN, NIL and NIN), with the complete ranking in Table 10. The rolling standard-deviation classification is no longer among them, since it has been removed for the data-format reasons given in our response to Comment 1.6.

Changes to the manuscript: Table 3 (contingency); Table 6 (marginal effects); Tables 5 and S1 (all 18 permutations).

Comment 1.43. *Lines 456-457: I think the circumstance is not solely related to the exponent being close to 1. At mid-frequency ranges, the dependence of the gamma-R coefficient on microphysical properties is less pronounced.*

Response: We agree and have revised the passage accordingly; the Discussion now attributes the mid-frequency insensitivity to both aspects: "*At those frequencies the exponent of the γ-R relation is close to unity and the retrieval is only weakly sensitive to the coefficients (Chwala and Kunstmann, 2019). For these frequencies, our local fits are also close to the ITU recommendation.*" This is consistent with the revised calibration: at 25 GHz the exponent is close to unity, the two local fitting strategies are nearly identical, and the local and ITU relations are closest, whereas the differences between the local and ITU relations grow towards the low and high frequencies, where the sensitivity to the drop size distribution is stronger (Sect. 4.4, Fig. 4 and Table 4).

Comment 1.44. *As noted in my general comments, the Discussion and Conclusions sections partially overlap and could be better distinguished.*

Response: Addressed; see our response to Comment 1.4. The Discussion has been rewritten into three thematic subsections (previous nationwide retrievals; assumptions and limitations; operational implications), and the summary of findings now resides exclusively in the Conclusions.

We once more thank the reviewer for the exceptionally constructive review, which has led, in our opnion, to a substantially stronger manuscript.

1 Figures

Note that original Figure 2 was removed, since the frequency-length distribution is now shown in Figure 7a and b for a representative sample of links.

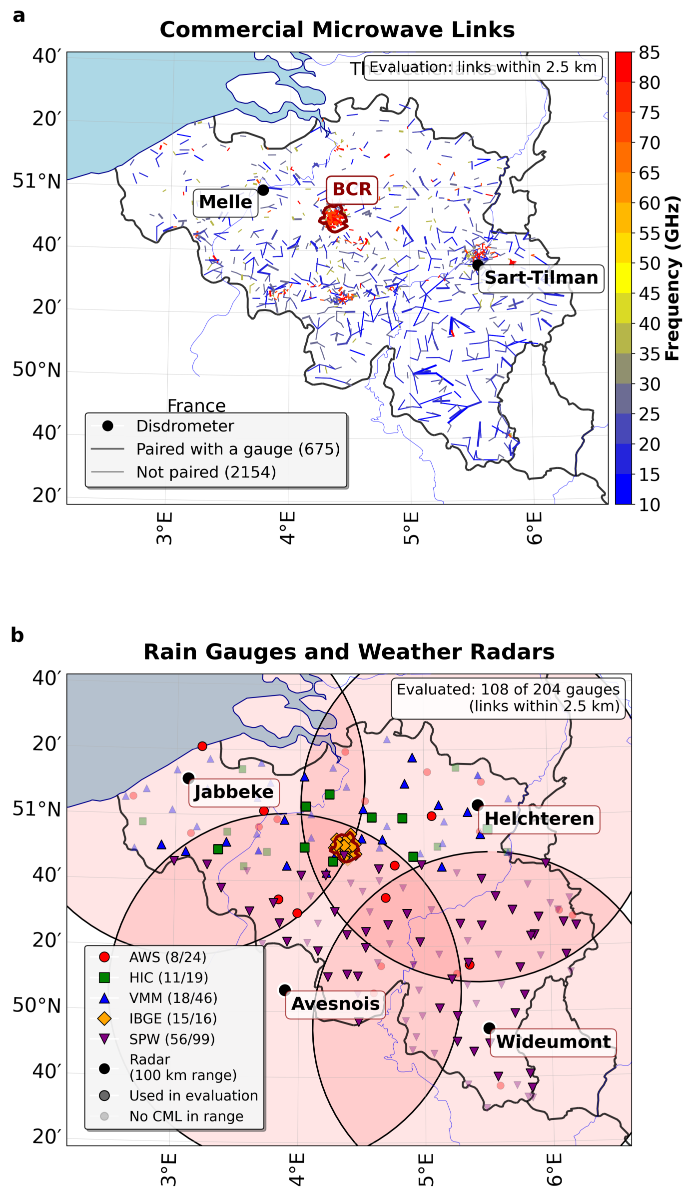

Figure 1: Spatial distribution of (a) CML network and disdrometers and (b) rain-gauge and weather radar networks in Belgium as used in this study. The colors of the CMLs reflect their operating frequency. The rain-gauge networks have different symbols as outlined in the legend. A 100 km radius around each radar site is shown by the black circles. The red outline of the Brussels-Capital Region (BCR) is also shown, for reference (see Section 4.6).Rain gauges highlighted in (b) are within 2.5 km of a CML midpoint, and are the ones used in the more detailed evaluation of CML-rainfall permutations and RAD-QPE

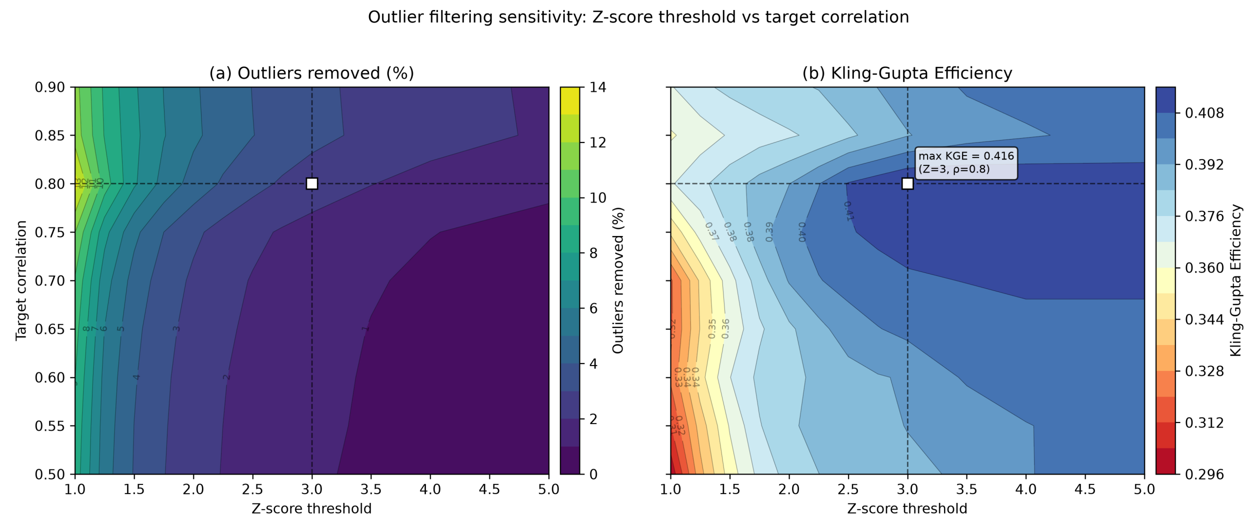

Figure 2: Sensitivity of the outlier filter (Section 3.2) to the Z-score threshold Z_{thr} and the target correlation ρ^*: (a) percentage of 15-min link samples removed and (b) Kling–Gupta efficiency (Equation 15) of the retrieved 15-min rainfall evaluated against the rain gauges. Both quantities are averaged over all four cases and all 18 processing permutations (72 retrieval runs). The white square and dashed lines mark the selected combination ($Z_{\mathrm{thr}} = 3$, $\rho^* = 0.8$), for which the mean KGE reaches its maximum of 0.416.

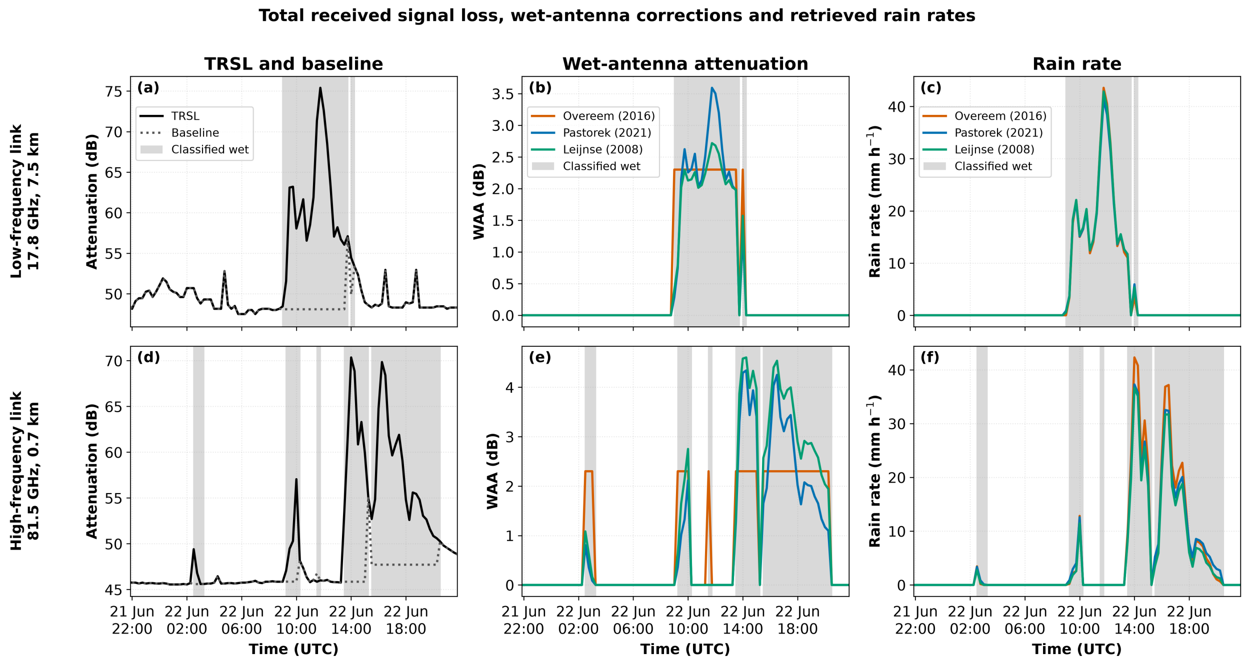

Figure 3: Time series for a low-frequency link (17.8 GHz, 7.5 km; top row) and a high-frequency link (81.5 GHz, 0.7 km; bottom row) for Case 1. Shown are (a, d) the total received signal loss (TRSL) and the retrieved baseline attenuation A_{dry}, (b, e) the wet-antenna attenuation A_{waa} and (c, f) the retrieved 15-min rain rates, for the constant correction of Overeem et al. (2016a) (·C·, orange), the intensity-dependent correction of Pastorek et al. (2022) (·I·, blue) and the intensity- and frequency-dependent correction of Leijnse et al. (2008) (·F·, green). Grey shading indicates the intervals classified as wet by the radar-based classification, which is shared by all three permutations.

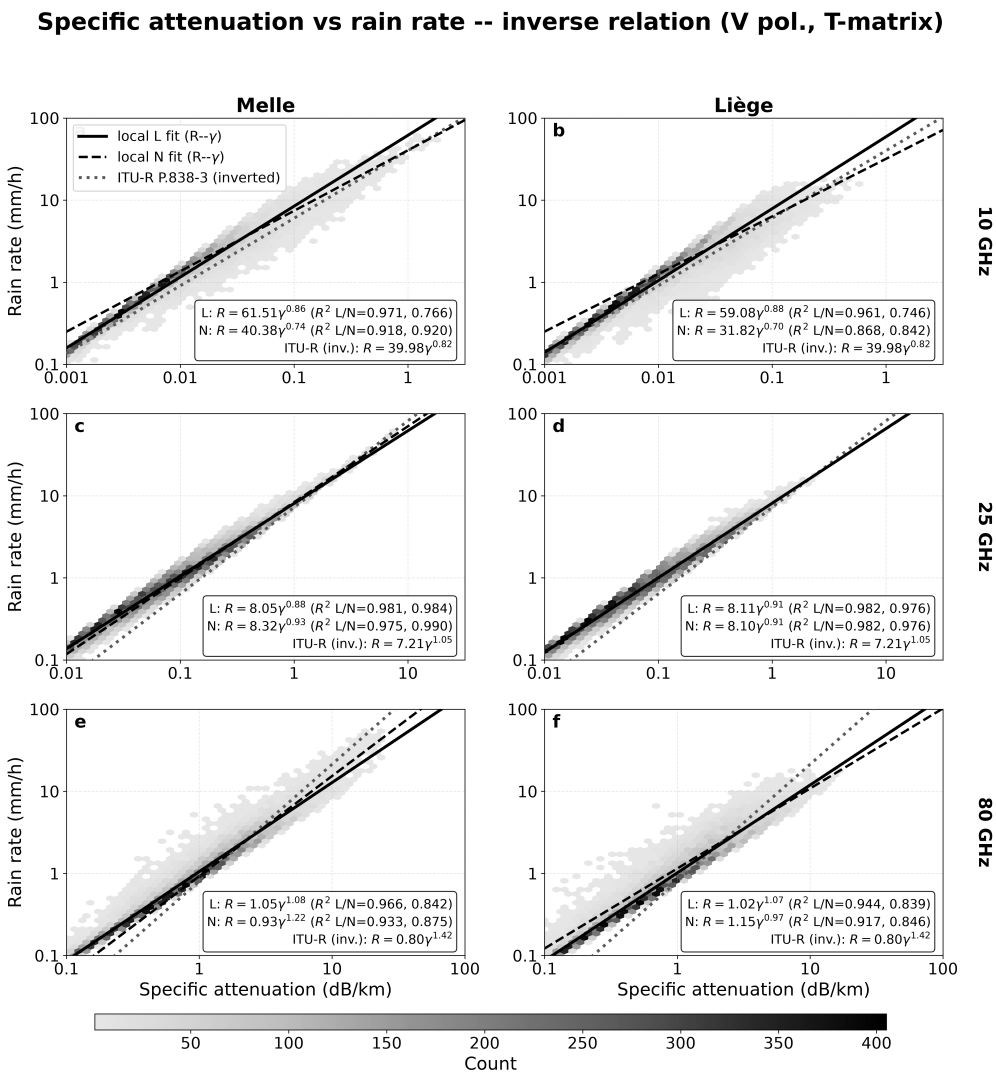

Figure 4: Rain rate as a function of specific attenuation for the (left) Melle and (right) Liège disdrometers at (top) 10 GHz, (middle) 25 GHz and (bottom) 80 GHz, assuming vertical polarization, based on the one-minute observations of May–September 2024 and 2025. The greyscale indicates the number of observations per bin. The dotted line shows the inverted ITU relation (ITU, 2005), the dashed line the local non-linear fit and the solid line the local fit in log–log space, all in the retrieval direction $\mathrm{R} = \mathrm{a}\,\gamma^{\mathrm{b}}$. The boxes list the fitted coefficients of both local relations, with their coefficients of determination evaluated in logarithmic and in linear space, together with the inverted ITU relation. Note the different X-axis ranges for each frequency.

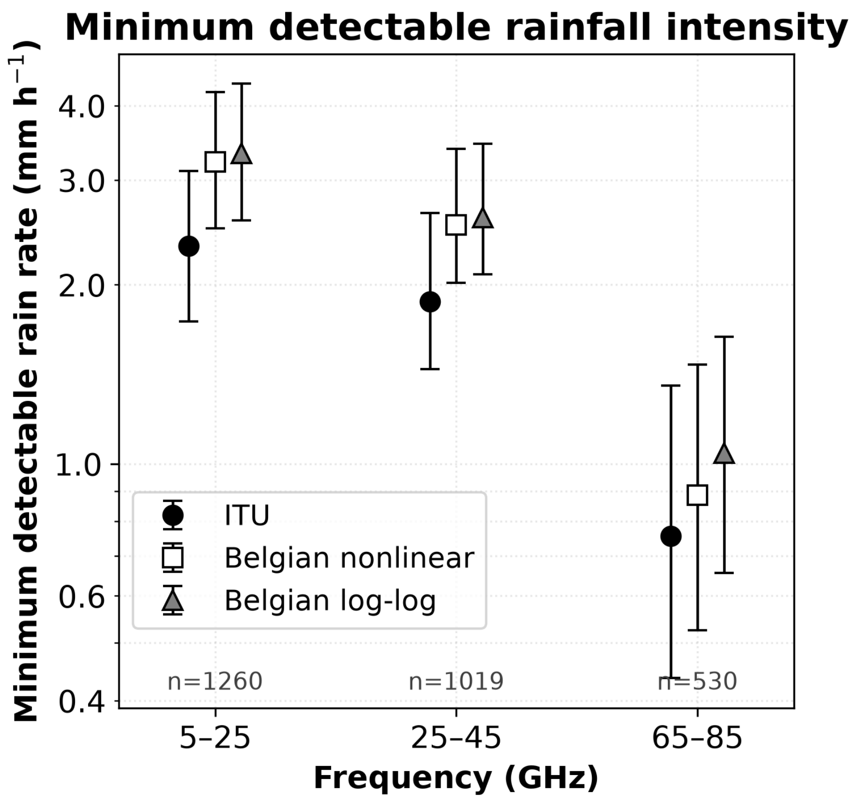

Figure 5: Minimum detectable rain rate implied by the 1 dB quantization of the network management system, computed for each individual sublink as $R_{\min} = (\Delta A_{\mathrm{q}}/(a'L))^{1/b'}$, with $\Delta A_{\mathrm{q}} = 1$ dB, L the path length and a' and b' the attenuation-form coefficients ($a' = a^{-1/b}$) corresponding to the frequency and polarization of the sublink. Results are grouped in three frequency bands, using the ITU relation (ITU, 2005) and the two Belgian relations obtained from the combined disdrometer observations. Symbols denote the median and the whiskers the interquartile range of the sublinks within each band, with the number of sublinks indicated at the bottom of the figure. The spread within a band is dominated by the distribution of path lengths. Note the logarithmic vertical axis and that no links are present between 45 and 65 GHz.

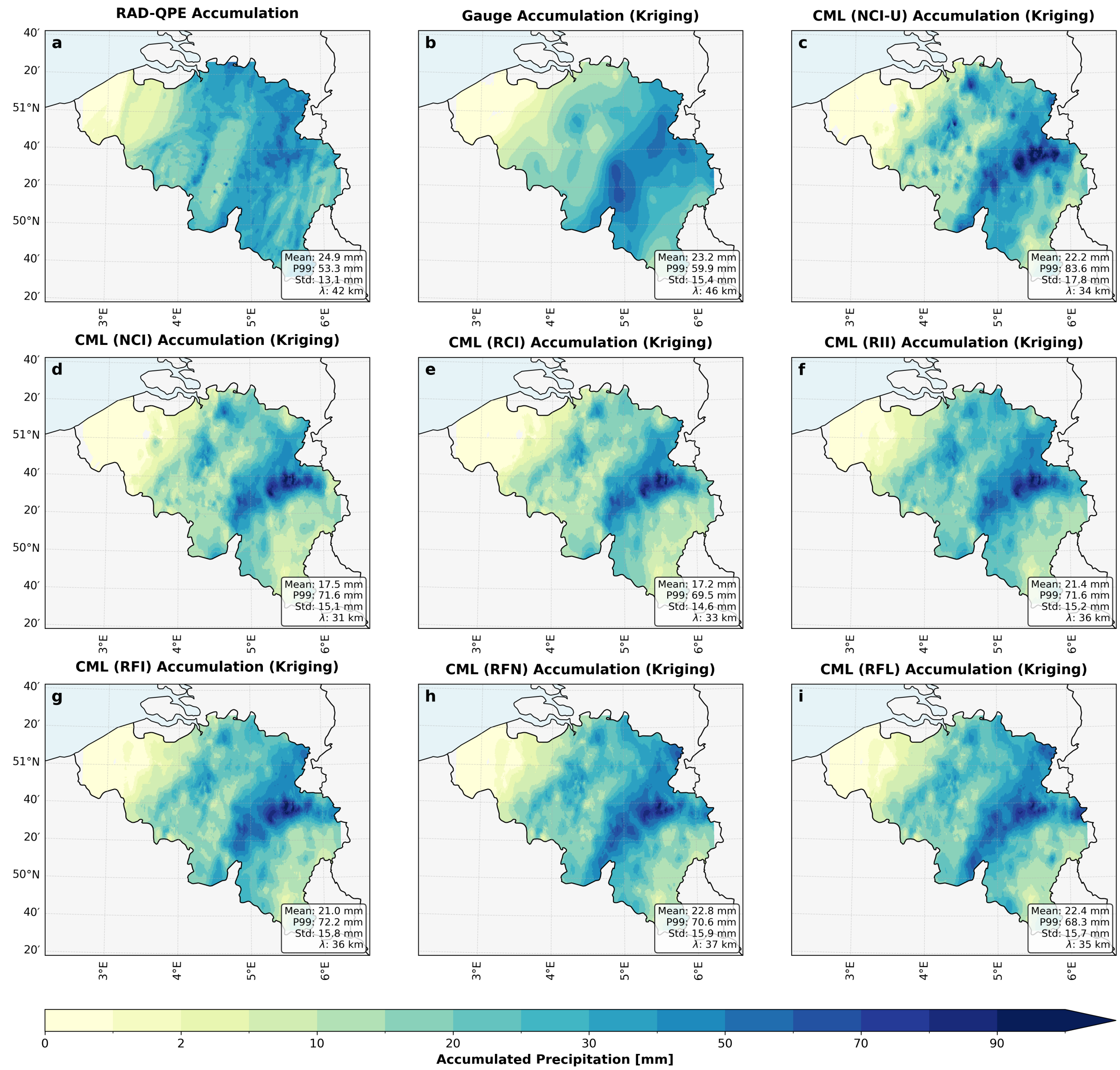

Figure 6: Accumulated rainfall during Case 1 from (a) RAD-QPE, (b) the rain gauges and (c–i) seven CML retrieval permutations, with the gauge and CML accumulations interpolated to the 1-km RAD-QPE grid using ordinary kriging (Section 2.3) and each CML treated as a point measurement at its midpoint. The permutations successively alter one processing step: outlier filtering (c, d), wet–dry classification (d, e), wet-antenna correction (e, f, g) and γ–R relation (g, h, i). The box in each panel lists the spatial mean, the 99th percentile (P99), the standard deviation (Std) and the autocorrelation length scale λ, computed as the e-folding radius of the radially averaged 2D autocorrelation. Corresponding maps for Cases 2 to 4 are provided in the supplementary material.

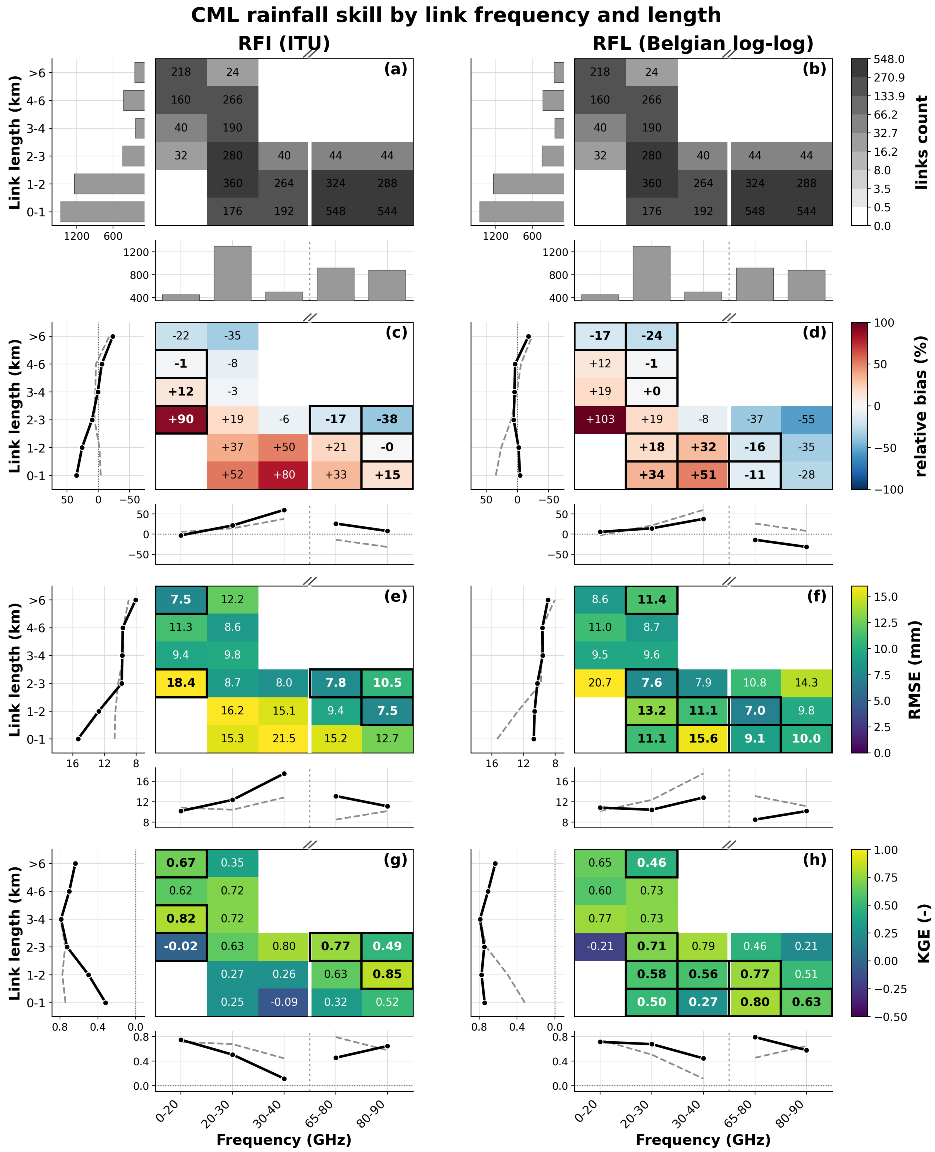

Figure 7: Per-link agreement with rain gauges as a function of link frequency (columns) and path length (rows), for the ITU relation (RFI, left column) and the Belgian log–log relation (RFL, right column). Panel rows show the number of gauge–CML pairs (a, b), relative bias (c, d), RMSE (e, f), and KGE (g, h), with a shared colour scale for RFI and RFL. Marginal profiles summarize each metric by pooling across frequency bins (left) or path-length bins (bottom), weighted by the number of pairs; KGE is recomputed from the pooled samples because it cannot be averaged across bins. In the metric marginals, the solid black line shows the experiment of the corresponding column and the dashed grey line the other experiment; count marginals are identical for both experiments and are shown as grey bars. The 45–65 GHz range contains no links and is omitted, and links ≥6 km are pooled into the top row. In the relative bias, RMSE, and KGE panels, the better-performing experiment in each bin is highlighted by a bold outline and value (relative bias: smaller absolute value). Statistics are computed for individual gauge–link pairs within a 2.5-km matching radius.

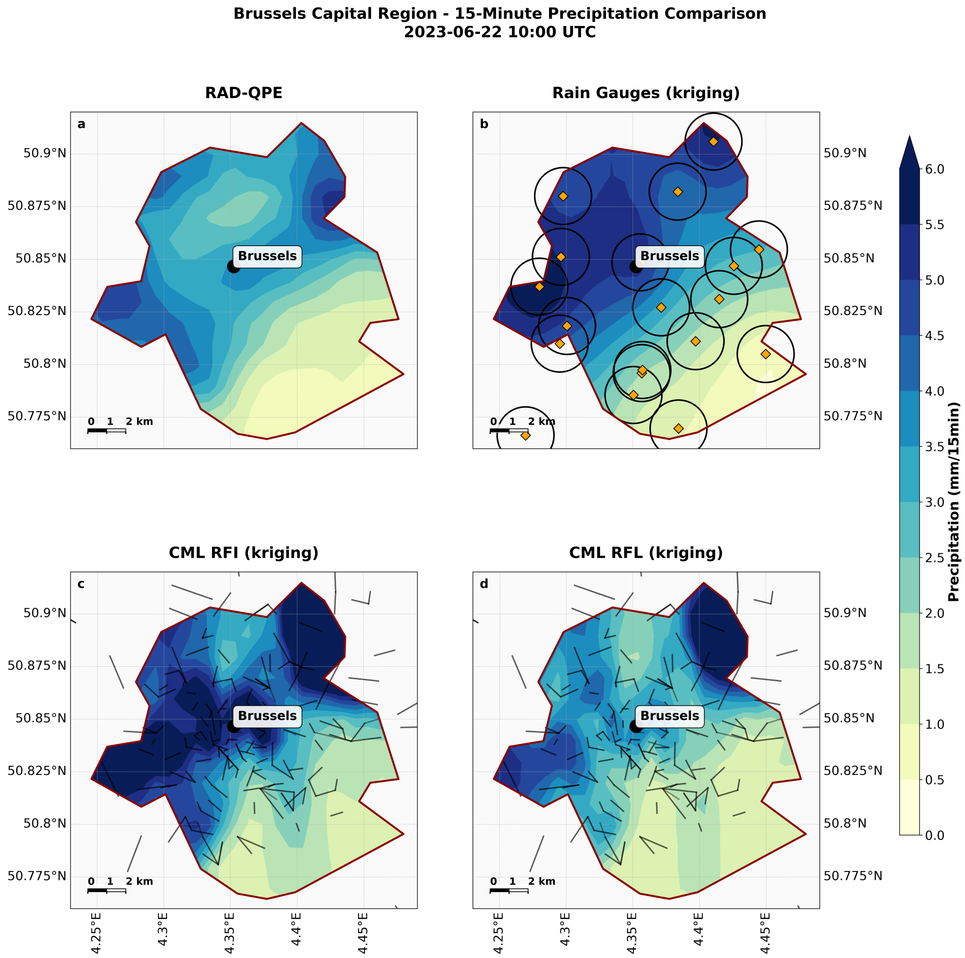

Figure 8: 15-min rainfall accumulation at 10:00 UTC on 22 June 2023 over the Brussels Capital Region (BCR), as obtained from (a) RAD-QPE, (b) the IBGE rain gauge network, (c) the RFI CML retrieval and (d) the RFL CML retrieval. Only data within the BCR are shown and the brown outline denotes its border. All data are regridded to the 1-km RAD-QPE grid using ordinary kriging. Gauge locations are indicated in panel b by orange diamonds, with a radius of 1 km drawn around them to focus on data that are not extrapolated too far from the gauges. Panels c and d also show the locations of all CMLs in the BCR.

2 Tables

Table 1: General statistics of case-accumulated precipitation across all 204 rain gauges shown in Figure 1 and for all cases. Shown are the case Duration, Mean Accumulations (Acc), 99th Percentile of the case-accumulations (P99) and the Standard Deviation of the accumulations (Std) across all stations.

Case	Duration	Acc (mm)	P99 (mm)	Std (mm)
Case 1	22 June 2023 (24 hours)	21.5	55.2	14.8
Case 2	8-9 July 2023 (48 hours)	3.0	15.7	3.4
Case 3	23-24 July 2023 (48 hours)	20.1	47.6	14.0
Case 4	28-29 July 2023 (48 hours)	10.5	46.3	10.3

Table 2: Naming convention of the CML rainfall retrieval permutations. Each permutation is identified by a three-letter acronym combining one option from each of the three processing steps (e.g., RIL = radar-based wet–dry classification, intensity-dependent wet-antenna correction, log–log Belgian $\gamma - \mathrm{R}$ relation). The suffix -U denotes retrievals without the outlier filtering of Section 3.2 (all other permutations are outlier-filtered). See text for details.

Position	Letter	Method	Reference
1 (Wet–Dry Classification)	N	Nearby links	Overeem et al. (2016a)
	R	Radar-based (RAD-QPE)	similar to Overeem et al. (2011)
2 (Wet-Antenna Correction)	C	Constant (2.3 dB)	Overeem et al. (2016a)
	I	Intensity-dependent	Pastorek et al. (2022)
	F	Frequency- and intensity-dependent	Leijnse et al. (2008)
3 ($\mathrm{R} - \gamma$ relation)	I	ITU recommendation	ITU (2005)
	N	Belgian disdrometers, nonlinear fit	Section **??**
	L	Belgian disdrometers, log–log fit	Section **??**
Suffix	-U	No outlier filtering (also retaining records with errored seconds)	Section **??**

Table 3: Comparison of wet/dry detection skill based on contingency table statistics for the Nearby Link approach (N) and the RAD-QPE approach (R). Shown are the number of samples (n), Probability of Detection (POD), False Alarm Ratio (FAR), Critical Success Index (CSI), Percent Correct (PC), and Heidke Skill Score (HSS). Values are provided per case, and for all cases combined. Higher values indicate better performance for POD, CSI, PC, and HSS, whereas lower values indicate better performance for FAR.

Case	Method	n	POD	FAR	CSI	PC	HSS
All cases	N	48128	0.74	0.53	0.41	0.87	0.50
	R	48128	0.57	0.35	0.43	0.91	0.56
Case 1	N	8648	0.89	0.40	0.56	0.91	0.66
	R	8648	0.85	0.35	0.58	0.92	0.69
Case 2	N	13160	0.70	0.71	0.26	0.97	0.40
	R	13160	0.72	0.67	0.29	0.97	0.44
Case 3	N	13160	0.80	0.58	0.38	0.84	0.47
	R	13160	0.56	0.35	0.43	0.91	0.55
Case 4	N	13160	0.65	0.52	0.38	0.77	0.40
	R	13160	0.45	0.26	0.39	0.85	0.47

Table 4: Overview of the R–γ relation parameters, a (mm h^{-1}(km dB^{-1})$^{\mathrm{b}}$) and b (unitless) (Equation 3), for the inverted ITU (2005) relation, as fitted directly to the combined observations of the two disdrometers in Belgium using the log–log and the non-linear fit, and as documented in Overeem et al. (2016a) for The Netherlands, for frequencies of 10, 25 and 80 GHz and vertical polarization. The Belgian and Dutch coefficients are directly comparable to parameters a and b in Figure 2 of Overeem et al. (2016a). Relations fitted to the individual disdrometers are reported in the panels of Figure 4.

	ITU (inv.)		Belgium (log–log)		Belgium (non-lin.)		Netherlands (non-lin.)	
Frequency	a	b	a	b	a	b	a	b
10 GHz	39.98	0.82	60.17	0.87	39.52	0.75	37.71	0.75
25 GHz	7.21	1.05	8.07	0.90	8.28	0.93	8.11	0.95
80 GHz	0.80	1.42	1.03	1.08	0.94	1.18	1.00	1.34

Table 5: The five best-performing CML permutations per case and combined over all cases, ranked by KGE and compared with RAD-QPE, evaluated against the case-accumulated rain gauge observations (Section 3.6). For the CMLs all links with midpoints within 2.5 km, and for RAD-QPE all pixels within 2.5 km of the gauge are averaged. Only gauges with valid data for all products are included (n samples). The complete ranking of all 18 permutations is provided in the supplementary material (Table 10).

Product	n	KGE (–)	Bias (mm)	Rel. bias (%)	RMSE (mm)	R^2 (–)	r (–)
All cases							
RFL	387	0.85	0.2	1.7	7.3	0.71	0.85
RFN	387	0.83	1.0	7.6	7.4	0.69	0.86
RCN	387	0.83	-1.0	-7.6	7.3	0.70	0.85
NCL	387	0.82	-0.7	-5.4	7.9	0.65	0.84
RIL	387	0.81	1.6	12.0	7.6	0.68	0.85
RAD-QPE	387	0.65	4.0	29.1	8.6	0.59	0.83
Case 1							
NCN	102	0.78	-0.9	-4.1	9.1	0.55	0.80
NCL	102	0.77	-2.0	-9.6	9.0	0.56	0.79
RCN	102	0.76	-2.0	-9.7	9.2	0.54	0.79
RFL	102	0.76	0.5	2.4	9.5	0.51	0.77
NFL	102	0.75	1.7	8.2	9.5	0.50	0.78
RAD-QPE	102	0.66	4.5	21.2	9.8	0.47	0.77
Case 2							
RCN	103	0.69	0.4	12.2	2.6	0.53	0.75
NCN	103	0.68	0.3	7.6	2.7	0.48	0.72
RCL	103	0.68	0.2	5.2	2.5	0.56	0.75
NCL	103	0.65	0.0	0.3	2.7	0.48	0.70
NCI	103	0.63	0.5	16.3	3.2	0.29	0.68
RAD-QPE	103	-1.40	7.1	213.6	9.1	-4.68	0.76
Case 3							
RCN	99	0.77	-0.9	-4.3	9.5	0.55	0.78
RFN	99	0.76	2.1	9.8	9.5	0.55	0.78
RFL	99	0.75	0.6	3.0	9.1	0.59	0.78
RCL	99	0.72	-2.5	-11.5	9.6	0.54	0.77
RIL	99	0.72	2.7	12.4	9.9	0.51	0.76
RAD-QPE	99	0.69	2.7	12.8	9.1	0.59	0.79
Case 4							
RIN	83	0.57	-0.5	-5.5	5.0	0.57	0.77
RIL	83	0.55	-0.8	-9.6	5.1	0.56	0.77
RFN	83	0.52	-0.9	-11.0	5.3	0.53	0.75
RII	83	0.50	-0.6	-6.9	5.3	0.52	0.74
RFL	83	0.49	-1.3	-15.4	5.4	0.51	0.75
RAD-QPE	83	0.63	1.0	12.0	5.0	0.58	0.77

Table 6: Marginal effect of each processing choice, obtained by averaging the pooled evaluation metrics of Table S1 over all permutations sharing the respective option (N_{per} permutations each). Since the permutation set is a full 2×3×3 factorial, every option occurs equally often with all combinations of the other two factors, so that the averages are balanced. Options are ranked by mean KGE. Note that the values are mean scores across permutations rather than scores of a pooled product.

Option	N_{per}	KGE (–)	Bias (mm)	|Rel. bias| (%)	RMSE (mm)	R^2 (–)
Wet/dry classification						
Radar	9	0.785	0.68	9.6	7.89	0.653
Nearby link	9	0.598	2.31	18.1	10.29	0.401
Wet antenna attenuation						
Overeem 2016 (constant)	6	0.756	-0.39	5.9	8.51	0.589
Leijnse 2008 (freq./intensity)	6	0.704	1.74	12.7	8.96	0.542
Pastorek 2021 (intensity)	6	0.614	3.14	23.0	9.80	0.449
R-γ relation						
Belgium log-log	6	0.751	0.87	12.5	8.24	0.617
Belgium non-linear	6	0.712	1.62	14.4	8.78	0.562
ITU	6	0.611	2.00	14.7	10.25	0.402

Table 7: As Table 1, but for the IBGE network only, and including the average rain rates. Shown are the domain-average rain rate (mm h^{-1}), averaged over all 15-min intervals of the case, including the dry ones; the domain-average intensity (mm h^{-1}), averaged over the wet intervals only, that is, conditional on rainfall being recorded; the case-total accumulation (mm) and the case-accumulated 99th percentile (mm) and standard deviation (mm). The mean rate therefore reflects both the intensity and the temporal occurrence of rainfall, whereas the mean intensity characterises the rainfall when it occurs.

Case	Mean Rate (mm h^{-1})	Mean Intensity (mm h^{-1})	Mean Accumulation (mm)	P99 (mm)	Std (m
Case 1	1.08	5.3	26.0	33.7	7.9
Case 2	0.11	6.5	5.4	13.0	3.2
Case 3	0.79	6.0	37.9	42.4	3.3
Case 4	0.11	4.8	5.1	7.7	1.6
Overall	0.44	5.7	18.6	42.3	14.7

Table 8: The five best-performing CML permutations per case and combined over all cases, ranked by KGE and compared with RAD-QPE, evaluated against the 15-minute rainfall observations of the IBGE network in the BCR. For each gauge, the CML retrievals are averaged over all links with midpoints within 1 km, and RAD-QPE is taken as the average of the grid points within the same radius. n_{sam} denotes the number of 15-minute samples pooled over all gauges. The complete ranking of all 18 permutations is provided in the supplementary material (Table 11).

Product	n_{sam}	KGE (–)	Bias (mm/15 min)	Rel. bias (%)	RMSE (mm/15 min)	R^2 (–)	r (–)
All cases							
RFL	7073	0.83	0.005	4.2	0.283	0.68	0.84
RCL	7073	0.81	-0.007	-5.5	0.295	0.65	0.82
RIL	7073	0.80	0.017	13.8	0.269	0.71	0.85
RCN	7073	0.76	0.007	6.1	0.329	0.57	0.82
RFN	7073	0.76	0.017	14.1	0.308	0.62	0.83
RAD-QPE	7073	0.66	0.024	19.6	0.381	0.42	0.74
Case 1							
NCN	1047	0.88	0.011	3.5	0.372	0.80	0.90
RCN	1047	0.86	-0.024	-7.4	0.363	0.81	0.90
RFN	1047	0.84	0.032	10.1	0.384	0.79	0.89
NCL	1047	0.79	-0.015	-4.7	0.379	0.79	0.89
RFL	1047	0.79	0.012	3.7	0.394	0.78	0.88
RAD-QPE	1047	0.72	0.064	20.1	0.372	0.80	0.90
Case 2							
RCL	2208	0.62	0.003	13.2	0.193	0.28	0.65
RFL	2208	0.62	0.004	17.6	0.183	0.36	0.67
NCL	2208	0.62	0.004	16.1	0.193	0.29	0.65
NFL	2208	0.61	0.005	21.1	0.183	0.36	0.67
RIL	2208	0.56	0.007	30.4	0.177	0.40	0.69
RAD-QPE	2208	-2.10	0.059	249.0	0.501	-3.81	0.76
Case 3							
RIL	2024	0.84	0.014	7.0	0.331	0.72	0.86
RFL	2024	0.83	0.005	2.5	0.362	0.66	0.84
RCL	2024	0.80	-0.004	-2.1	0.391	0.60	0.82
RIN	2024	0.72	0.038	18.3	0.374	0.64	0.86
RFN	2024	0.70	0.030	14.4	0.413	0.56	0.83
RAD-QPE	2024	0.69	-0.026	-12.4	0.338	0.70	0.84
Case 4							
RIL	1794	0.53	0.001	4.5	0.165	0.06	0.70
RFL	1794	0.38	0.002	8.0	0.188	-0.22	0.70
RIN	1794	0.36	0.004	15.2	0.187	-0.22	0.70
RCL	1794	0.27	0.003	10.2	0.205	-0.46	0.69
RFN	1794	0.16	0.005	20.6	0.218	-0.65	0.69
RAD-QPE	1794	0.10	0.012	44.4	0.232	-0.86	0.57

3 Review Tables and Figures

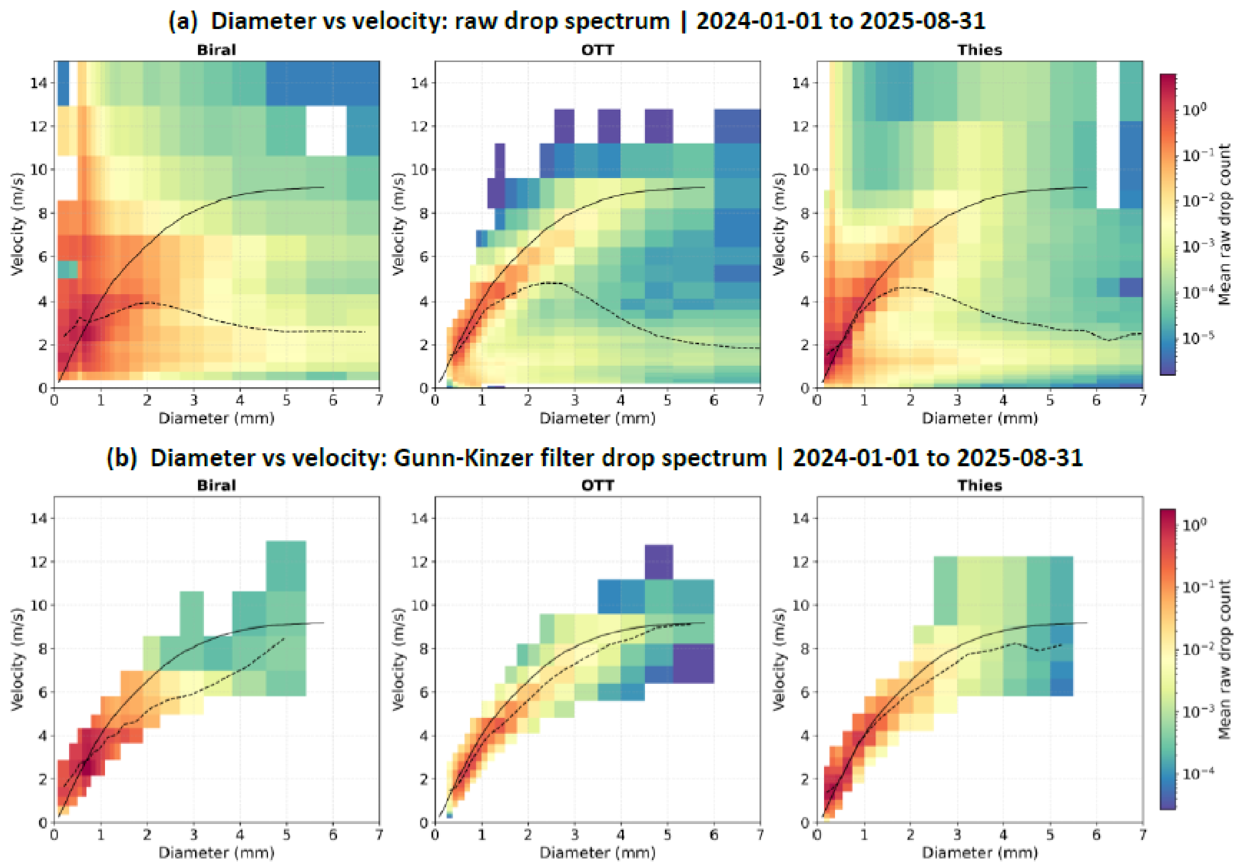

Figure 9: Raw (a) and filterd (b) drop spectra of the three disdrometers in Belgium (left: Biral in Uccle; middle: OTT Parsivel in Melle; right: Thies Climate in Sart Tilman). The population of low-velocity/ large diameter particles in all disdrometers are snowflakes, which are filtered out. The Biral disdrometer has a very large number of particles with small diameters and high velocitity as well, and no clear rain signature like the other two disdrometers.

Table 9: Sensitivity of the evaluation to the gauge–CML pairing rule. Each row repeats the full evaluation of all 18 processing permutations for one pairing rule: the radius-mean rules average all links whose midpoint lies within the stated radius of the gauge, while the last row pairs each gauge with its single nearest link and discards gauges whose nearest link lies further than 5 km. The 2.5 km row is the configuration used in the manuscript. The left-hand block scores each pairing rule on its own set of matched gauges, whose size n (the number of case-combined gauge samples over the four cases) necessarily grows with the radius; the right-hand block repeats the exercise on the $n_{\text{fix}} = 126$ samples that all pairing rules have in common, so that the estimator can be compared at constant sample. *Best permutation* is the three-letter code of the permutation with the highest KGE under that pairing, and *KGE*, *Rel. bias* and *RMSE* characterise that best permutation. The two radar columns give the corresponding RAD-QPE benchmark on the same gauges, sampled in two ways: *RAD-QPE (point)* takes the single radar grid point nearest to the gauge and is therefore independent of the CML pairing, so that any variation down that column reflects only the changing station set; *RAD-QPE (area)* averages the radar over the same radius as the CMLs and therefore shares their spatial support. On the common sample the point radar is by construction identical for every row (KGE = 0.73) and is omitted from the right-hand block. The area-averaged radar is not meaningful for the nearest-link rule, where it would average radar over 5 km against a single link, and that value should be disregarded.

	Own matched gauges							Common gauges ($n_{\text{fix}} = 126$)		
		Best permutation				RAD-QPE		Best perm.		RAD-QPE
Pairing rule	n	Code	KGE (–)	Rel. bias (%)	RMSE (mm)	point (–)	area (–)	Code	KGE (–)	area (–)
Radius mean, 1 km	126	RCL	0.82	−10.8	8.25	0.73	0.73	RCL	0.82	0.73
Radius mean, 1.5 km	224	RFL	0.87	−1.5	7.42	0.72	0.72	RCN	0.84	0.73
Radius mean, 2 km	326	RFL	0.85	−0.4	7.30	0.68	0.68	RCN	0.89	0.73
Radius mean, 2.5 km	387	RFL	0.85	1.7	7.29	0.65	0.65	RCN	0.91	0.73
Radius mean, 3 km	445	RFL	0.82	2.0	7.94	0.66	0.66	RCN	0.91	0.73
Radius mean, 5 km	638	RFN	0.83	7.2	7.80	0.67	0.66	RCN	0.90	0.72
Radius mean, 10 km	773	RFI	0.83	6.4	7.83	0.67	0.65	NCL	0.91	0.70
Nearest link, ≤5 km	664	RFL	0.73	3.9	10.53	0.68	0.67	RCL	0.75	0.72

4 Supplementary Material

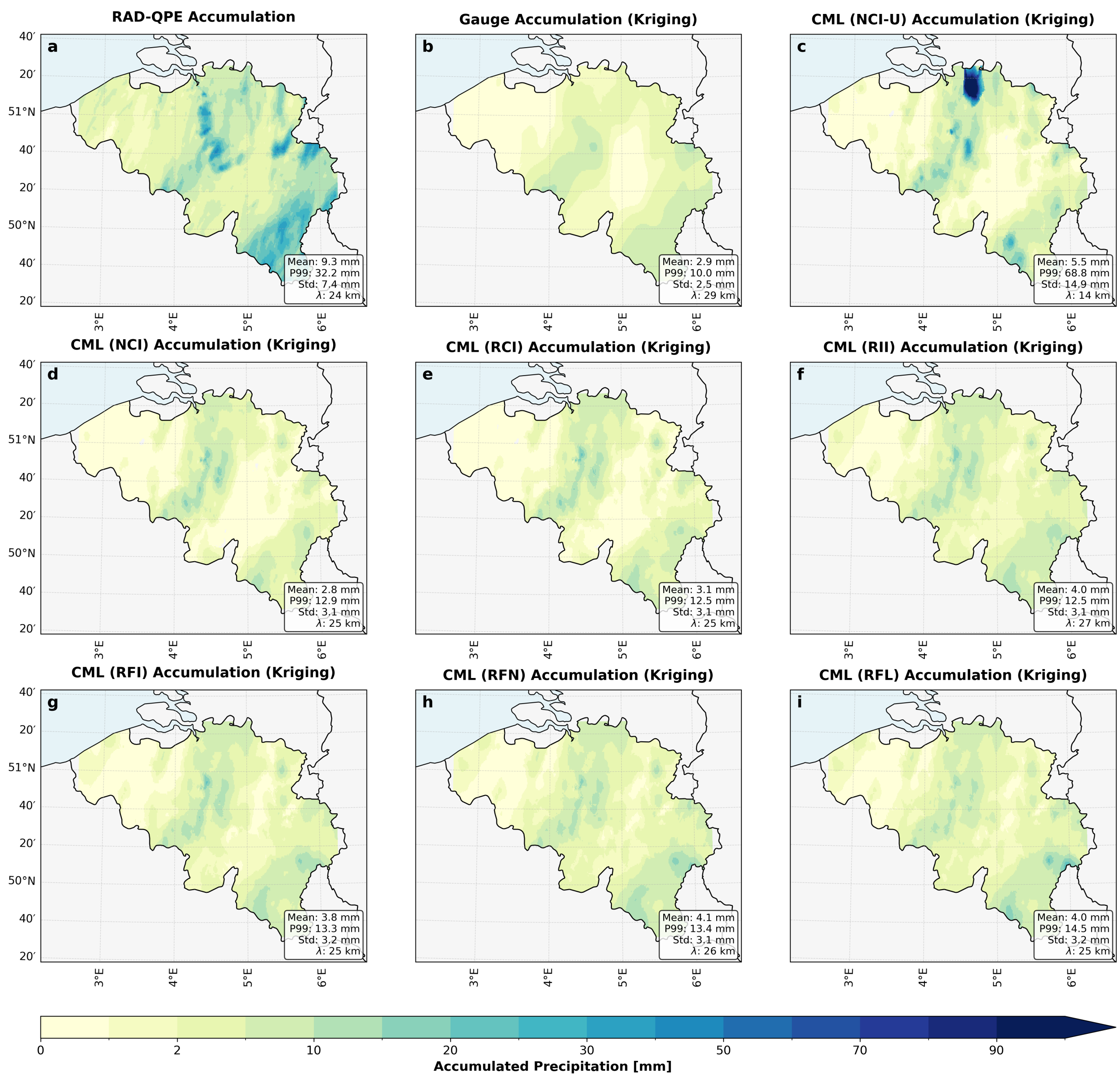

Figure 10: As Figure 6, but for case 2.

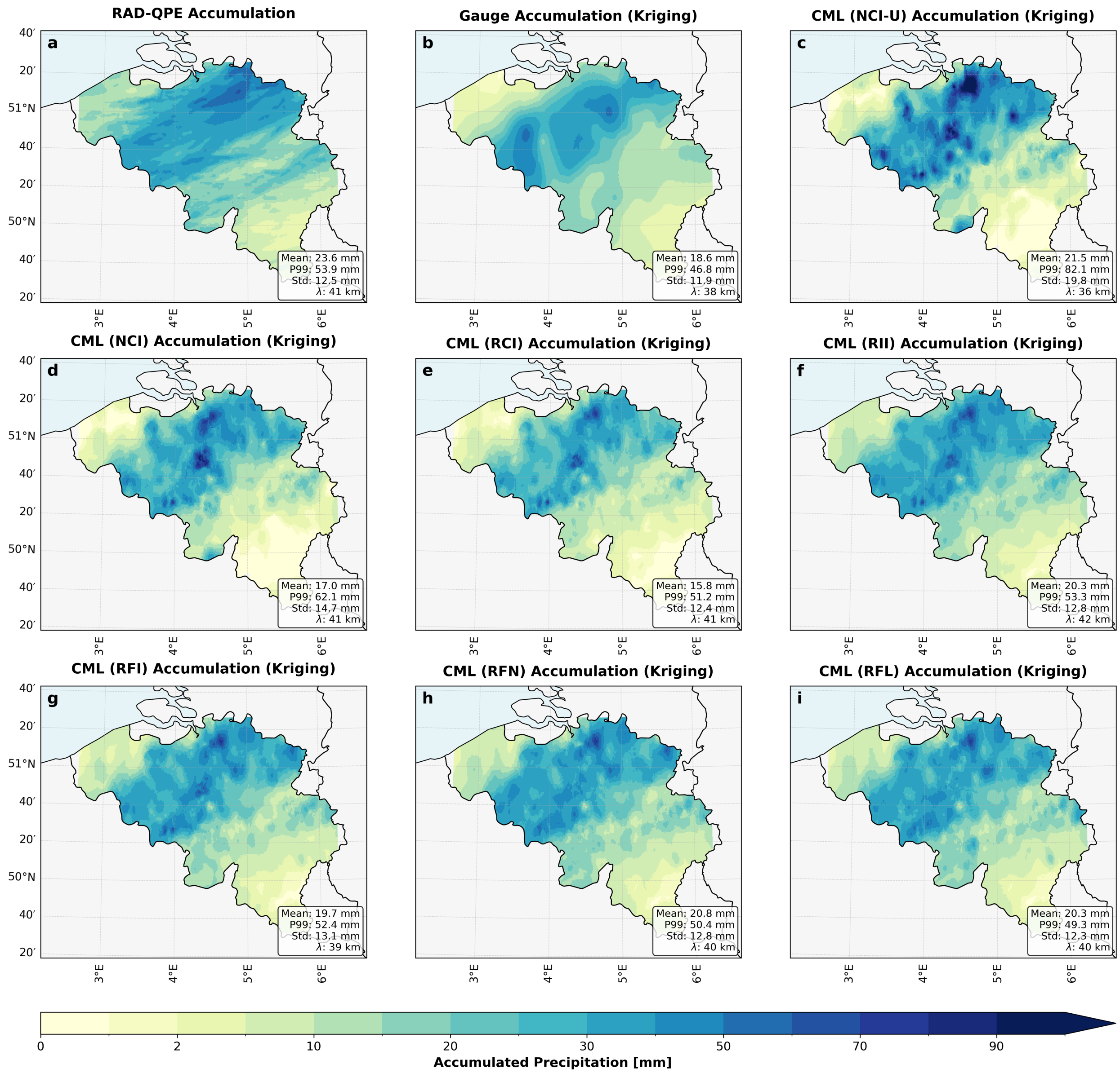

Figure 11: As Figure 6, but for case 3.

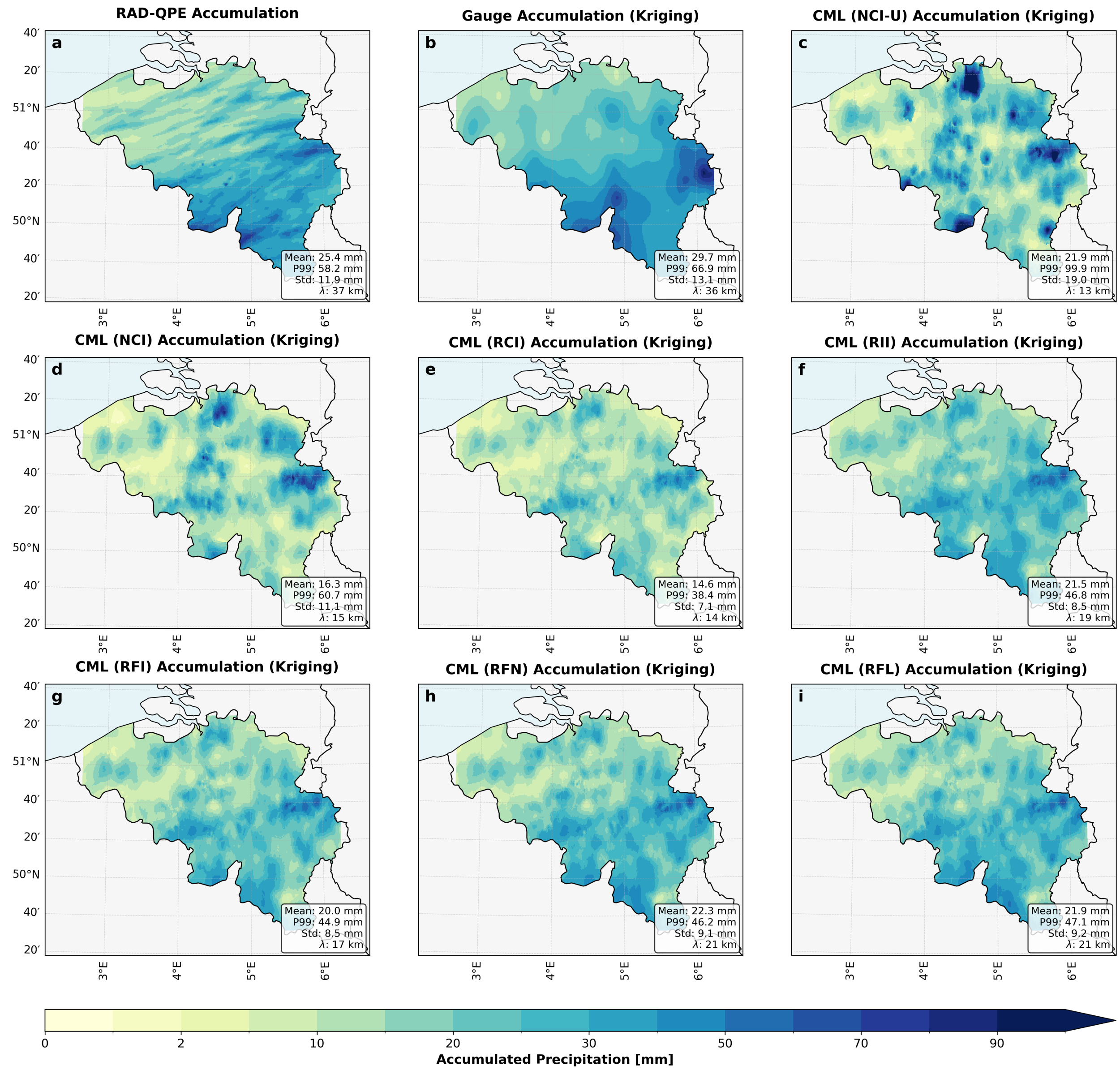

Figure 12: As Figure 6, but for case 4.

Table 10: As Table 5, but for the complete ranking of all 18 permutations.

Product	n	KGE (–)	Bias (mm)	Rel. bias (%)	RMSE (mm)	R^2 (–)	r (–)
All cases							
RFL	387	0.85	0.2	1.7	7.3	0.71	0.85
RFN	387	0.83	1.0	7.6	7.4	0.69	0.86
RCN	387	0.83	-1.0	-7.6	7.3	0.70	0.85
NCL	387	0.82	-0.7	-5.4	7.9	0.65	0.84
RIL	387	0.81	1.6	12.0	7.6	0.68	0.85
RCL	387	0.77	-1.8	-13.1	7.4	0.70	0.85
NCN	387	0.77	0.2	1.1	8.6	0.59	0.83
RCI	387	0.77	0.0	0.1	8.7	0.58	0.83
RIN	387	0.76	2.3	16.8	8.0	0.65	0.85
RFI	387	0.76	1.4	10.0	8.4	0.61	0.85
NFL	387	0.70	2.1	15.1	9.0	0.55	0.84
RII	387	0.70	2.4	17.3	8.9	0.56	0.85
NFN	387	0.60	2.8	20.5	10.0	0.44	0.84
NCI	387	0.57	1.1	7.8	11.1	0.31	0.80
NIL	387	0.56	3.8	27.7	10.3	0.42	0.84
NFI	387	0.49	2.9	21.4	11.6	0.25	0.82
NIN	387	0.48	4.5	32.7	11.3	0.30	0.84
NII	387	0.38	4.3	31.5	12.8	0.09	0.81
RAD-QPE	387	0.65	4.0	29.1	8.6	0.59	0.83
Case 1							
NCN	102	0.78	-0.9	-4.1	9.1	0.55	0.80
NCL	102	0.77	-2.0	-9.6	9.0	0.56	0.79
RCN	102	0.76	-2.0	-9.7	9.2	0.54	0.79
RFL	102	0.76	0.5	2.4	9.5	0.51	0.77
NFL	102	0.75	1.7	8.2	9.5	0.50	0.78
RCL	102	0.75	-2.9	-13.7	9.2	0.54	0.79
RFN	102	0.74	1.6	7.5	9.6	0.50	0.79
RIL	102	0.73	3.1	14.8	9.8	0.47	0.78
NFN	102	0.71	2.8	13.1	10.0	0.45	0.79
RFI	102	0.70	1.1	5.2	10.1	0.44	0.79
RCI	102	0.70	-1.7	-7.8	10.4	0.41	0.77
RIN	102	0.68	3.8	18.3	10.4	0.40	0.78
NCI	102	0.68	-0.4	-1.8	10.6	0.39	0.77
NIL	102	0.67	4.4	21.0	10.6	0.38	0.77
NFI	102	0.65	2.4	11.4	10.9	0.35	0.78
RII	102	0.63	3.1	14.5	11.5	0.27	0.75
NIN	102	0.62	5.3	25.2	11.4	0.29	0.78
NII	102	0.55	4.7	22.4	12.7	0.12	0.74
RAD-QPE	102	0.66	4.5	21.2	9.8	0.47	0.77
Case 2							
RCN	103	0.69	0.4	12.2	2.6	0.53	0.75

NCN	103	0.68	0.3	7.6	2.7	0.48	0.72
RCL	103	0.68	0.2	5.2	2.5	0.56	0.75
NCL	103	0.65	0.0	0.3	2.7	0.48	0.70
NCI	103	0.63	0.5	16.3	3.2	0.29	0.68
RCI	103	0.62	0.7	22.0	3.2	0.30	0.70
RFL	103	0.61	0.8	23.5	2.6	0.52	0.75
NFL	103	0.60	0.8	22.7	3.0	0.39	0.69
NFN	103	0.59	0.9	27.8	3.0	0.37	0.70
RFN	103	0.58	1.0	31.2	2.8	0.44	0.74
NFI	103	0.57	1.0	29.8	3.2	0.27	0.69
RFI	103	0.56	1.1	33.8	3.1	0.33	0.72
RIL	103	0.53	1.2	34.9	2.8	0.47	0.76
NIL	103	0.52	1.2	35.7	3.1	0.31	0.69
RIN	103	0.51	1.3	40.4	2.9	0.41	0.74
RII	103	0.49	1.4	41.6	3.2	0.27	0.71
NII	103	0.48	1.3	40.0	3.4	0.19	0.68
NIN	103	0.48	1.4	41.1	3.3	0.25	0.68
RAD-QPE	103	-1.40	7.1	213.6	9.1	-4.68	0.76
Case 3							
RCN	99	0.77	-0.9	-4.3	9.5	0.55	0.78
RFN	99	0.76	2.1	9.8	9.5	0.55	0.78
RFL	99	0.75	0.6	3.0	9.1	0.59	0.78
RCL	99	0.72	-2.5	-11.5	9.6	0.54	0.77
RIL	99	0.72	2.7	12.4	9.9	0.51	0.76
RIN	99	0.71	4.0	18.6	10.4	0.46	0.77
NCL	99	0.68	1.3	5.9	10.8	0.42	0.79
RFI	99	0.61	3.8	17.6	11.6	0.33	0.80
RII	99	0.59	5.1	23.8	11.7	0.32	0.81
RCI	99	0.56	2.1	9.8	12.0	0.28	0.80
NCN	99	0.54	3.1	14.3	12.5	0.22	0.78
NFL	99	0.47	6.4	30.1	13.4	0.11	0.81
NFN	99	0.33	7.9	36.9	15.8	-0.23	0.78
NIL	99	0.33	9.3	43.6	15.9	-0.25	0.79
NIN	99	0.20	10.8	50.3	17.8	-0.57	0.79
NCI	99	0.15	5.7	26.6	17.8	-0.57	0.77
NFI	99	0.09	8.8	41.3	18.9	-0.78	0.78
NII	99	-0.01	11.1	52.1	20.5	-1.09	0.79
RAD-QPE	99	0.69	2.7	12.8	9.1	0.59	0.79
Case 4							
RIN	83	0.57	-0.5	-5.5	5.0	0.57	0.77
RIL	83	0.55	-0.8	-9.6	5.1	0.56	0.77
RFN	83	0.52	-0.9	-11.0	5.3	0.53	0.75
RII	83	0.50	-0.6	-6.9	5.3	0.52	0.74
RFL	83	0.49	-1.3	-15.4	5.4	0.51	0.75
RFI	83	0.49	-0.8	-10.3	5.5	0.50	0.73
RCN	83	0.44	-1.7	-21.3	5.6	0.47	0.75
NIL	83	0.44	-0.4	-4.9	6.4	0.31	0.56

NFN	83	0.44	-0.9	-11.3	6.3	0.32	0.58
RCI	83	0.43	-1.3	-16.2	5.9	0.42	0.68
NFL	83	0.43	-1.1	-13.7	6.3	0.33	0.59
RCL	83	0.41	-2.1	-25.8	5.7	0.45	0.76
NIN	83	0.41	-0.3	-3.1	6.6	0.27	0.53
NFI	83	0.37	-1.1	-13.5	6.8	0.22	0.51
NII	83	0.35	-0.7	-8.3	6.9	0.18	0.47
NCL	83	0.33	-2.5	-30.4	6.6	0.26	0.61
NCN	83	0.32	-2.2	-26.9	6.8	0.22	0.55
NCI	83	0.27	-2.0	-24.5	7.3	0.11	0.44
RAD-QPE	83	0.63	1.0	12.0	5.0	0.58	0.77

Table 11: As Table 8, but for the complete ranking of all 18 permutations.

Product	n	KGE (–)	Bias (mm/15 min)	Rel. bias (%)	RMSE (mm/15 min)	R^2 (–)	r (–)
All cases							
RCL	8133	0.77	-0.003	-2.7	0.315	0.57	0.77
RFL	8133	0.77	0.008	6.5	0.311	0.58	0.78
RIL	8133	0.73	0.019	16.1	0.306	0.59	0.79
RCN	8133	0.73	0.010	8.9	0.346	0.48	0.77
RFN	8133	0.71	0.020	16.8	0.336	0.51	0.78
RIN	8133	0.65	0.031	26.4	0.329	0.53	0.79
NCL	8133	0.64	0.027	23.3	0.360	0.44	0.75
NFL	8133	0.50	0.049	42.3	0.357	0.45	0.76
NCN	8133	0.48	0.043	36.8	0.406	0.29	0.75
NIL	8133	0.36	0.068	58.2	0.356	0.45	0.77
RFI	8133	0.36	0.047	40.7	0.451	0.12	0.76
NFN	8133	0.35	0.063	54.2	0.398	0.32	0.76
RII	8133	0.31	0.059	50.6	0.434	0.19	0.78
RCI	8133	0.27	0.048	40.8	0.501	-0.08	0.75
NIN	8133	0.23	0.081	69.7	0.389	0.34	0.77
NFI	8133	-0.01	0.090	77.1	0.528	-0.21	0.75
NCI	8133	-0.02	0.080	69.0	0.575	-0.43	0.73
NII	8133	-0.09	0.106	90.7	0.500	-0.08	0.76
RAD-QPE	8133	0.68	0.023	19.5	0.349	0.47	0.77
Case 1							
RCN	1141	0.84	0.010	3.7	0.401	0.72	0.85
NCL	1141	0.79	0.018	6.2	0.402	0.72	0.85
NCN	1141	0.78	0.044	15.4	0.417	0.70	0.85
RCL	1141	0.78	-0.011	-3.8	0.392	0.73	0.85
RFL	1141	0.74	0.045	15.9	0.402	0.72	0.85
RFN	1141	0.72	0.066	23.3	0.410	0.71	0.85
NFL	1141	0.68	0.070	24.8	0.412	0.70	0.84
NFN	1141	0.64	0.092	32.5	0.420	0.69	0.85
RCI	1141	0.62	0.059	20.9	0.518	0.53	0.85
RIL	1141	0.60	0.098	34.5	0.432	0.67	0.83
RFI	1141	0.59	0.094	33.2	0.475	0.60	0.86
RIN	1141	0.55	0.120	42.2	0.437	0.67	0.84
NCI	1141	0.51	0.101	35.5	0.545	0.48	0.84
NIL	1141	0.49	0.132	46.4	0.461	0.63	0.82
NFI	1141	0.45	0.136	47.8	0.510	0.55	0.85
NIN	1141	0.42	0.157	55.2	0.474	0.61	0.83
RII	1141	0.39	0.157	55.2	0.495	0.57	0.86
NII	1141	0.22	0.204	72.0	0.548	0.47	0.84
RAD-QPE	1141	0.65	0.087	30.6	0.392	0.73	0.86
Case 2							
NCN	2392	0.58	0.003	9.9	0.236	0.27	0.61
RCN	2392	0.58	0.003	8.8	0.236	0.27	0.60

RFN	2392	0.58	0.003	11.9	0.229	0.31	0.62
NFN	2392	0.57	0.004	14.9	0.231	0.30	0.61
NCL	2392	0.56	-0.001	-1.8	0.224	0.34	0.61
NFL	2392	0.56	0.001	4.8	0.221	0.36	0.62
RIL	2392	0.55	0.002	7.3	0.217	0.38	0.63
RCL	2392	0.55	-0.001	-4.7	0.223	0.35	0.61
RIN	2392	0.55	0.006	20.9	0.229	0.31	0.62
RFL	2392	0.54	-0.000	-0.1	0.221	0.36	0.61
NIL	2392	0.53	0.004	14.5	0.222	0.35	0.61
NIN	2392	0.53	0.007	25.0	0.230	0.31	0.62
NFI	2392	0.39	0.012	40.7	0.281	-0.04	0.58
RFI	2392	0.38	0.012	40.7	0.283	-0.05	0.58
RII	2392	0.35	0.014	47.5	0.275	0.00	0.59
NII	2392	0.32	0.015	51.1	0.275	0.00	0.59
NCI	2392	0.32	0.013	43.6	0.303	-0.20	0.57
RCI	2392	0.29	0.014	46.9	0.307	-0.24	0.57
RAD-QPE	2392	-1.04	0.046	158.7	0.415	-1.27	0.87
Case 3							
RIL	2392	0.78	0.014	6.8	0.391	0.59	0.79
RFL	2392	0.77	0.003	1.5	0.412	0.55	0.77
RCL	2392	0.76	-0.005	-2.5	0.424	0.52	0.76
RFN	2392	0.69	0.028	13.5	0.457	0.44	0.77
RIN	2392	0.69	0.038	18.4	0.432	0.50	0.79
RCN	2392	0.67	0.023	11.4	0.479	0.39	0.76
NCL	2392	0.50	0.072	35.3	0.509	0.31	0.75
NFL	2392	0.35	0.113	55.0	0.504	0.32	0.77
NCN	2392	0.28	0.106	51.7	0.594	0.06	0.75
NIL	2392	0.27	0.137	66.9	0.486	0.37	0.78
RII	2392	0.24	0.100	49.0	0.617	-0.02	0.77
RFI	2392	0.22	0.093	45.2	0.654	-0.14	0.75
NFN	2392	0.15	0.143	69.9	0.583	0.09	0.76
NIN	2392	0.09	0.165	80.5	0.551	0.19	0.77
RCI	2392	0.08	0.105	51.1	0.731	-0.43	0.74
NII	2392	-0.30	0.215	105.1	0.747	-0.49	0.76
NFI	2392	-0.31	0.201	98.0	0.806	-0.74	0.74
NCI	2392	-0.35	0.187	91.5	0.878	-1.06	0.73
RAD-QPE	2392	0.69	-0.024	-11.5	0.342	0.69	0.83
Case 4							
RIL	2208	0.52	0.001	2.8	0.180	-0.08	0.57
RFL	2208	0.47	0.001	3.6	0.192	-0.23	0.56
RCL	2208	0.45	0.001	2.5	0.195	-0.27	0.57
RIN	2208	0.41	0.004	14.5	0.201	-0.34	0.56
RFN	2208	0.34	0.004	15.0	0.213	-0.52	0.56
RCN	2208	0.27	0.005	17.1	0.224	-0.67	0.57
NCL	2208	0.07	0.013	46.2	0.242	-0.94	0.55
RII	2208	-0.05	0.012	42.9	0.267	-1.37	0.55
NFL	2208	-0.06	0.021	75.7	0.230	-0.77	0.56

RFI	2208	-0.16	0.013	44.5	0.286	-1.71	0.55
NCN	2208	-0.17	0.018	61.6	0.273	-1.49	0.55
NIL	2208	-0.19	0.028	99.5	0.216	-0.56	0.56
NFN	2208	-0.25	0.025	88.3	0.256	-1.18	0.55
NIN	2208	-0.34	0.031	110.1	0.236	-0.86	0.55
RCI	2208	-0.42	0.016	56.5	0.323	-2.47	0.56
NII	2208	-0.59	0.034	118.7	0.286	-1.72	0.54
NFI	2208	-0.65	0.030	105.9	0.321	-2.43	0.54
NCI	2208	-0.77	0.027	94.1	0.359	-3.28	0.54
RAD-QPE	2208	-0.06	0.014	48.8	0.237	-0.88	0.72

References

Beard, K. V.: Terminal Velocity and Shape of Cloud and Precipitation Drops Aloft, Journal of Atmospheric Sciences, 33, 851 – 864, https://doi.org/10.1175/1520-0469(1976)033<0851:TVASOC>2.0.CO;2, 1976.

Berne, A. and Uijlenhoet, R.: Path-averaged rainfall estimation using microwave links: Uncertainty due to spatial rainfall variability, Geophysical Research Letters, 34, https://doi.org/https://doi.org/10.1029/2007GL029409, 2007.

Bertrand, C., Ingels, R., and Journée, M.: Homogenization and trends analysis of the Belgian historical precipitation time series, International Journal of Climatology, 41, 5277–5294, https://doi.org/https://doi.org/10.1002/joc.7129, 2021.

Blettner, N., Fencl, M., Bareš, V., Kunstmann, H., and Chwala, C.: Transboundary Rainfall Estimation Using Commercial Microwave Links, Earth and Space Science, 10, e2023EA002 869, https://doi.org/https://doi.org/10.1029/2023EA002869, 2023.

Bringi, V. N., Chandrasekar, V., Hubbert, J., Gorgucci, E., Randeu, W. L., and Schoenhuber, M.: Raindrop Size Distribution in Different Climatic Regimes from Disdrometer and Dual-Polarized Radar Analysis, Journal of the Atmospheric Sciences, 60, 354 – 365, https://doi.org/10.1175/1520-0469(2003)060<0354:RSDIDC>2.0.CO;2, 2003.

Chwala, C. and Kunstmann, H.: Commercial microwave link networks for rainfall observation: Assessment of the current status and future challenges, WIREs Water, 6, e1337, https://doi.org/https://doi.org/10.1002/wat2.1337, e1337 WATER-363.R2, 2019.

Delvaux, C., Ingels, R., Vrábeĺ, V., Journée, M., and Bertrand, C.: Quality control and homogenization of the Belgian historical temperature data, International Journal of Climatology, 39, 157–171, https://doi.org/https://doi.org/10.1002/joc.5792, 2019.

Ghiggi, G., Candolfi, K., Billaux-Roux, A.-C., Longchamps, R., Pham-Ba, S., Weil, C., and Berne, A.: disdrodb: an open-source Python package for standardized processing, sharing, and analysis of disdrometer data, EGUsphere, 2026, 1–71, https://doi.org/10.5194/egusphere-2026-1886, 2026.

Graf, M., Chwala, C., Polz, J., and Kunstmann, H.: Rainfall estimation from a German-wide commercial microwave link network: optimized processing and validation for 1 year of data, Hydrology and Earth System Sciences, 24, 2931–2950, https://doi.org/10.5194/hess-24-2931-2020, 2020.

Graf, M., Wagner, A., Polz, J., Lliso, L., Lahuerta, J. A., Kunstmann, H., and Chwala, C.: Improved rain event detection in commercial microwave link time series via combination with MSG SEVIRI data, Atmospheric Measurement Techniques, 17, 2165–2182, https://doi.org/10.5194/amt-17-2165-2024, 2024.

ITU: Recommendation ITU-R P.838-3, Specific attenuation model for rain for use in prediction methods, Tech. rep., International Telecommunication Union, https://www.itu.int/dms$_pubrec/itu-r/rec/p/R-REC-P.838-3-200503-I!!PDF-E.pdf$, 2005.

Journée, M., Goudenhoofdt, E., Vannitsem, S., and Delobbe, L.: Quantitative rainfall analysis of the 2021 mid-July flood event in Belgium, Hydrology and Earth System Sciences, 27, 3169–3189, https://doi.org/10.5194/hess-27-3169-2023, 2023.

Leijnse, H., Uijlenhoet, R., and Stricker, J.: Microwave link rainfall estimation: Effects of link length and frequency, temporal sampling, power resolution, and wet antenna attenuation, Advances in Water Resources, 31, 1481–1493, https://doi.org/https://doi.org/10.1016/j.advwatres.2008.03.004, 2008.

Overeem, A., Leijnse, H., and Uijlenhoet, R.: Measuring urban rainfall using microwave links from commercial cellular communication networks, Water Resources Research, 47, https://doi.org/https://doi.org/10.1029/2010WR010350, 2011.

Overeem, A., Leijnse, H., and Uijlenhoet, R.: Country-wide rainfall maps from cellular communication networks, Proceedings of the National Academy of Sciences, 110, 2741–2745, https://doi.org/10.1073/pnas.1217961110, 2013.

Overeem, A., Leijnse, H., and Uijlenhoet, R.: Retrieval algorithm for rainfall mapping from microwave links in a cellular communication network, Atmospheric Measurement Techniques, 9, 2425–2444, https://doi.org/10.5194/amt-9-2425-2016, 2016a.

Overeem, A., Leijnse, H., and Uijlenhoet, R.: Two and a half years of country-wide rainfall maps using radio links from commercial cellular telecommunication networks, Water Resources Research, 52, 8039–8065, https://doi.org/https://doi.org/10.1002/2016WR019412, 2016b.

Pastorek, J., Fencl, M., Rieckermann, J., and Bareš, V.: Precipitation Estimates From Commercial Microwave Links: Practical Approaches to Wet-Antenna Correction, IEEE Transactions on Geoscience and Remote Sensing, 60, 1–9, https://doi.org/10.1109/TGRS.2021.3110004, 2022.

Pu, K., Liu, X., and He, H.: Wet Antenna Attenuation Model of E-Band Microwave Links Based on the LSTM Algorithm, IEEE Antennas and Wireless Propagation Letters, 19, 1586–1590, https://doi.org/10.1109/LAWP.2020.3011463, 2020.

Roversi, G., Alberoni, P. P., Fornasiero, A., and Porcù, F.: Commercial microwave links as a tool for operational rainfall monitoring in Northern Italy, Atmospheric Measurement Techniques, 13, 5779–5797, https://doi.org/10.5194/amt-13-5779-2020, 2020.

Schleiss, M. and Berne, A.: Identification of Dry and Rainy Periods Using Telecommunication Microwave Links, IEEE Geoscience and Remote Sensing Letters, 7, 611–615, https://doi.org/10.1109/LGRS.2010.2043052, 2010.

Schleiss, M., Rieckermann, J., and Berne, A.: Quantification and Modeling of Wet-Antenna Attenuation for Commercial Microwave Links, IEEE Geoscience and Remote Sensing Letters, 10, 1195–1199, https://doi.org/10.1109/LGRS.2012.2236074, 2013.

Valtr, P., Fencl, M., and Bareš, V.: Excess Attenuation Caused by Antenna Wetting of Terrestrial Microwave Links at 32 GHz, IEEE Antennas and Wireless Propagation Letters, 18, 1636–1640, https://doi.org/10.1109/LAWP.2019.2925455, 2019.

van de Beek, C., Leijnse, H., Torfs, P., and Uijlenhoet, R.: Seasonal semi-variance of Dutch rainfall at hourly to daily scales, Advances in Water Resources, 45, 76–85, https://doi.org/https://doi.org/10.1016/j.advwatres.2012.03.023, space-Time Precipitation from Urban Scale to Global Change, 2012.

van het Schip, T. I., Overeem, A., Leijnse, H., Uijlenhoet, R., Meirink, J. F., and van Delden, A. J.: Rainfall measurement using cell phone links: classification of wet and dry periods using geostationary satellites, Hydrological Sciences Journal, 62, 1343–1353, https://doi.org/10.1080/02626667.2017.1329588, 2017.

van Leth, T. C., Overeem, A., Leijnse, H., and Uijlenhoet, R.: A measurement campaign to assess sources of error in microwave link rainfall estimation, Atmospheric Measurement Techniques, 11, 4645–4669, https://doi.org/10.5194/amt-11-4645-2018, 2018.

Vereecken, H., Cornet, E., Van Eerdenbruch, K., and Mostaert, F.: HIC – Hydrologisch Informatiecentrum – Verzamelen en verspreiden van meetgegevens, in: Congres Watersysteemkennis 2006–2007: Oppervlaktewaterkwantiteit, pp. 1–5, Waterbouwkundig Laboratorium, Departement Mobiliteit en Openbare Werken, https://www.vliz.be/imisdocs/publications/130633.pdf, 2007.